Optimization of MoP/r-GO Based Hybrids for Electrochemical Water Splitting

By

Rafiq Ur Rehman

School of Chemical and Materials Engineering

National University of Sciences and Technology

2022

Optimization of MoP/r-GO Based Hybrids for Electrochemical Water Splitting

Name: Rafiq Ur Rehman

Registration No: 00000327650

This thesis is submitted as a partial fulfilment of the requirements for the degree of

MS in Chemical Engineering

Supervisor Name: Dr. Erum Pervaiz

School of Chemical and Materials Engineering (SCME)

National University of Science and Technology (NUST)

H-12, Islamabad, Pakistan

December, 2022

Dedication

By the grace of Almighty Allah, Who is the Most Beneficent and the Most Merciful

This study is dedicated to my parents, who have always been my source of guidance and support.

To my supervisor who shared her knowledge, gave advice, and encouraged me to fulfill my objectives.

And to all my fellows I worked with, I've enjoyed wonderful memories.

Acknowledgments

There is none other but Almighty Allah, whose will is required for everything and anything in this world, who blessed us with the ability to think and made us willing to explore the entire universe. Infinite greetings to the Holy Prophet Muhammad (PBUH), the cause of the universe's creation and a fountain of knowledge and blessing for all humanity.

Dr. Erum Pervaiz, my renowned supervisor, deserves credit for trusting in my talents. His constant guidance, encouragement, and support were vital in the project's success. Author Erum Pervaiz acknowledges NUST Pakistan for providing its research facilities and HEC project marked (2017/HEC/NRPU-10482) for financial assistance.

I'd like to express my gratitude to my deserving GEC members, Dr. Muhammad Bilal Khan, Dr. Tayyaba Noor, and Dr. Salman Raza Naqvi. I've never given it much thought. Having said that, the unwavering moral support that my family and friends have always provided will always be my light in the dark. My heartfelt gratitude goes out to all the personnel and lab attendants. Thank you!

Rafiq Ur Rehman

Abstract

Hydrogen (H_2) production through water splitting has limited commercial applications due to the unfavorable kinetics of the reaction. Electrocatalysts with a robust structure, high levels of catalytic activity, and a high degree of stability are in high demand but challenging. A catalyst is generally needed for efficient electrocatalytic water-splitting. Long-term stability and high catalytic activity are the main obstacles in developing a catalyst for the hydrogen evolution reaction (HER). Water electrolysis is generally known as a more sustainable and viable technique of H_2 production than the stream reforming reaction due to its advantages of using water as a reactant, the absence of greenhouse gas emissions, and exceptional H_2 generation efficiency. Implementing low-cost water-splitting devices and electrolyzers could result in marketable H_2 fuel. Recently, Molybdenum Phosphide (MoP) has been found as a promising family of earth-abundant electrocatalysts for the HER. It has a wide range of compositions and structures, favorable electronic properties, and excellent electrical conductivity, resulting in low overpotentials at operationally relevant current densities and stability in extremely acidic environments. This study reports the synthesis of MoP/RGO-based hybrids electrocatalysts for HER. The optimized MoP/RGO-based hybrid electrocatalyst exhibited an exceptional HER electrocatalytic performance. An efficient MoP/RGO-based hybrid showed promising results. It exhibited an exceptional HER electrocatalytic performance having an overpotential of 96 mV, at a current density of 10 mA/cm^2, in an alkaline solution with a low Tafel slope of 64 mV/dec. The electrocatalyst also exhibited long-term stability with a minor potential decrease over 24 h. RGO is a promising material with high strength during the high-temperature phosphorization process preventing particle clumping and making the catalyst more conductive, improving the HER performance and durability of an electrocatalyst. Bifunctional MoP/RGO porous structure offered more electrolyte and ions transport permeability. The synergistic effect of reduced graphene oxide (RGO) doping with MoP improves electrocatalytic activity. A high electrocatalyst also exhibited long-term stability with a minor potential decrease over 24 h.

Table of Contents

List of Figures

List of Tables

Acronym

TOF: Turnover Frequency

MOF: Metallic Organic framework

FE: Faradaic Efficiency

OER: Oxygen evolution reaction

HER: Hydrogen evolution reaction

MoP: Molybdenum Phosphide

GO: Graphene oxide

RGO: Reduced graphene oxide

ECSA: Electrochemical active surface area

SEM: Scanning Electron Microscope

EDX: Energy-dispersive X-ray spectroscopy

FTIR: Fourier-Transform Infrared Spectroscopy

XRD: X-ray diffraction

Oxidation: Ox

Reduction: Red

dec^{-1}: Decade

Pt: Platinum

CV: Cyclic Voltammetry

LSV: Linear Sweep Voltammetry

EIS: Electrochemical Impedance Spectroscopy

Chapter 1

Introduction

1.1 Background

Climate change and the increasing global energy crisis are two major challenges for an advanced society. It is mandatory to develop viable clean energy carriers and energy conversion technologies to reduce greenhouse gas emissions and fossil fuel dependence. Hydrogen (H_2), like green energy and carbon-free carrier, keeps a more energy capacity, which is sponsored as an active nominee for the potential energy resources [1, 2]. Now, huge H_2 production mostly depends on the steam reforming reaction of fossil sources, which provokes the carbon footstep and reduction of fossil fuels [3-5]. Water electrolysis is generally known as a more sustainable and viable technique of H_2 production than the stream reforming reaction due to its advantages of using water as a reactant, the absence of greenhouse gas emissions, and exceptional H_2 generation efficiency [6-8].

Alternative electrocatalysts development has been necessary to lower manufacturing costs and increase HER performance. Transition metal phosphides with unique characteristics and a high earth abundance have received considerable attention in developing active electrocatalysts for HER [9-11]. Researchers have shown a significant interest in highly-active electrocatalysts containing common elements on the earth [12, 13]. It is critical to developing efficient and cost-effective HER electrocatalysts. Alternative electrocatalysts were required to reduce synthesis costs and improve HER performance. Because of their distinctive properties and high earth abundance, much research has been conducted to develop active HER electrocatalysts from Transition Metal Phosphide (TMPs). TMPs also have low costs and high catalytic activity [10]. Molybdenum Phosphide (MoP) has been identified as a strong candidate for HER catalysts. The transition metal MoP has realized significant benefits due to its different compositions and topologies, as well as its good electrical conductance and brilliant electronic properties [11]. On the other hand, the synthesis temperature for MoP is frequently greater than 700^{o}C, making it very easy to

sinter. As a result, obtaining well-crystallized nanostructured MoP remains challenging [14].

The kinetic hindrance of rate determining pathway, affects the catalytic activity of a catalyst in the HER. HER frequently involves multiple steps taking place on the electrode surface [15, 16]. The single-component catalyst's catalytic efficiency is limited because it cannot provide significant catalytic activity for all intermediate chemical reactions. Bimetallic electrocatalysts normally outperform single-component catalysts due to synergistic effects. An increase in active site composition and structural-dependent properties leads to increased overpotential and current density characteristics during water oxidation. Bimetallic cooperation and an open structure promote rapid electron mass flow and transmission. It is possible because there are many easily accessible catalytic sites [17]. Recently, several researchers demonstrated that the synergies of hybrid material boundaries could accelerate the entire HER mechanism, such as the incorporation of W_xC into WS_2 [18], Pt_3Ni to NiS [19], and NiS_2 to MoS_2 [20]. Such findings indicate that the rational design of hybrid catalysts is critical to improving the HER catalytic activity. In addition, by preparing MoP-based hybrids, performance of MoP based catalysts can be improved. MoP is efficient in the "H delivery" method because it achieves the lowest binding to H at a given Hydrogen coverage, showing the excellent HER catalyst [21].

As a result, MoP performs well in this role, and there has been an increase in interest in using it as an electrocatalyst for H_2 evolution. Most published articles, in contrast, emphasized the difficulty and significance of MoP preparation process. MoP had to be synthesized using a dual-step sintering procedure at a higher temperature in an N_2/H_2 or Ar/O_2 environment, resulting in a high cost and a complex operation [22, 23]. Enhancing the HER activity of MoP-based electrocatalysts in alkaline conditions is extremely difficult. RGO is an efficient support for fabricating effective hybrid electrocatalysts. The atomically fine 2D nanoarchitecture and outstanding electrical conductance of heterostructure facilitate both space-limited growth of well-scattered graphene and rapid interfacial electron transport. It allows uniformly dispersed nano catalysts to grow in small spaces [24, 25].

RGO has gained considerable interest as a favourable platform for enhanced electrocatalysts in various electrochemical conversion of energy activities. Its flexible service is mostly recognized for its unique chemical and physical properties, like excellent electronic structure, high specific surface area, and functionalization and structural modification [26, 27]. A simple hydrothermal technique produces N-doped molybdenum oxide, which is then annealed in an N_2 atmosphere and phosphorated to generate a sphere-shaped N-doped oxygenated MoP. The newly found N-doped phosphide structure improves HER catalytic performance by obtaining a low overpotential of about 87 mV at a current density of 10 mA/cm^2, which is better than the 138 mV overpotential of annealed N-doped molybdenum oxide in alkaline medium. Because of its large open surface, broad electrode/electrolyte interface, and reactant-specific binding energies, N-MoP is a particularly potent electrocatalyst for HER catalysis [28].

1.2 Fundamentals of Water Splitting Process

Break down of water into H_2 and O_2 has generated huge research attention as a viable method of obtaining sustainable and renewable energy [29, 30]. In a normal device for electrochemical water splitting, HER and OER are identical at cathode and anode, respectively. Fig. 1 shows the basic components of an OWS system. Depending on the electrolyte, which can be neutral (including seawater), alkaline or acidic, the OWS reaction and two half-reactions can be stated as follows [31, 32].

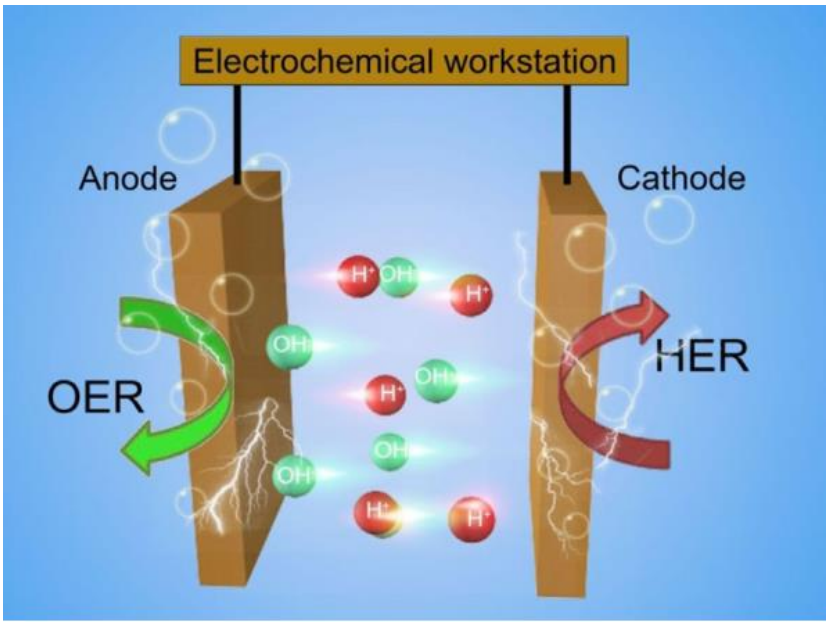

Figure 1: The diagram of the overall water splitting processes [33].

In acidic media

OER (Oxidation, Anode): $H_2O + 2e^- \rightarrow 0.5O_2 (\uparrow) + 2H^+$ E^o anode=1.23 V (1)

HER (Cathode, Reduction): $2H^+ + 2e^- \rightarrow H_2 (\uparrow)$ E^o cathode=0.00 V (2)

In neutral or alkaline media

OER (Oxidation, Anode): $2OH^- - 2e^- \rightarrow 0.5O_2(\uparrow) + 2H_2O$ E^o anode=1.23 V (3)

HER (Cathode, Reduction): $2H_2O + 2e^- \rightarrow H_2(\uparrow) + 2OH^-$ E^o cathode=0.00 V (4)

Overall reaction:

$$2H_2O \rightarrow O_2(\uparrow) + 2H_2(\uparrow) \quad (5)$$

The thermodynamics voltage value of electrocatalytic water splitting vs. RHE at 1atm and 25°C is 1.23 V, according to Eqn. (1–4). The additional voltage must be delivered to the cell in the study.

The overall cell voltage (V_{oc}) can be stated as

$$V_{oc}=1.23V+\eta_a+||\eta_c||+iR \quad (6)$$

Where η_c and η_a represent the cathodic and anodic overpotentials, and iR represents the ohmic drop. Therefore, a major effort must be put together to design particularly active catalysts that are cost-effective for the OER and HER in an electrolyze device to achieve H_2 economy by electrochemical water electrolysis [34].

1.3 Hydrogen Evolution Reaction

HER is a critical reaction for selecting electrochemical processes, which offers a vital link between energy conversion applications and renewable energy resources, i.e., reversible hydrogen fuel cells [35]. This HER needs high-performance electrocatalysts to speed up the decomposition of H_2O. A cathodic HER in aqueous acidic media takes place in the 2-electron-reaction model by an electrochemical "desorption step" and a "discharge step" [36]. The 1st step of the reaction is known as the Volmer reaction. Intermediate state of the H is produced by transferring an electron to one proton at the catalyst's surface. HER takes place at the cathode [37, 38].

The typical mechanism for HER in acidic media

$$e^- + H^+ + * \rightarrow H^* \qquad (7)$$

(Electrochemical adsorption, Volmer reaction, overpotential ≈120 mV/dec)

Then, two possible ways for the HER will go behind. First is Heyrovsky's reaction [39].

$$H^* + H^+ + e^- \rightarrow H_2 \qquad (8)$$

(Heyrovsky reaction, electrochemical desorption, ≈40 mV/dec)

The second is the Tafel recombination reaction [40].

$$H^* + H^* \rightarrow H_2 + 2^* \qquad (9)$$

(Tafel reaction, ≈30 mV/dec, chemical desorption)

In alkaline media

$$H_2O + e^- + * \rightarrow OH^- + H^* \quad (10)$$

(Volmer reaction, ≈120 mV/dec, electrochemical adsorption)

$$H_2O + H^* + e^- \rightarrow H_2 + OH^- \quad (11)$$

(Heyrovsky reaction, ≈40 mV/dec, electrochemical desorption)

$$H^* + H^* \rightarrow H_2 + 2^* \quad (12)$$

(Tafel reaction, ≈30 mV/dec, chemical desorption)

The * denotes the electrocatalyst's active site. Then adsorbed H atom on the surface of the electrocatalyst in the first Volmer step, forming the adsorbed hydrogen intermediate H*. Then, depending on the H atom's adsorption energy on the electrocatalyst surface, H* interacts with H^+ or H_2O (the Heyrovsky reaction) or with another recently formed H* (the Tafel reaction) in alkaline or acidic conditions to liberate one H_2 molecule [41]. In HER, the Volmer reaction is the fast reaction, and the other two reactions are the rate-limiting step. The Tafel slope determines a dominant mechanism. The critical parameter for the Tafel plot is to gain a low Tafel slope at a significant current density value. Tafel slope tells the overpotential of an electrochemical reaction. As much as lower the overpotential, there is an efficient HER electrocatalyst [42, 43]. In an acidic solution, the Volmer step relates to the electrochemical reduction of a proton to an adsorbed H. It is determined not only by the adsorption energy but also by the desorption of hydroxide ions (OH^-) and the dissociation of water in neutral and alkaline solutions.

1.4 Oxygen Evolution Reaction

OER is also another half-reaction for the overall water splitting reaction. Following reactions are involved in the OER mechanism in acidic media.

$$H_2O + * \rightarrow {}^*OH + e^- + H^+ \quad (13)$$

$$*OH \rightarrow {}^*O + e^- + H^+ \quad (14)$$

$$*O + H_2O \rightarrow *OOH + e^- + H^+ \quad (15)$$

$$*OOH \rightarrow O_2 + e^- + H^+ + * \quad (16)$$

The typical mechanism in neutral or alkaline media is below.

$$* + OH^- \rightarrow *OH + e^- \quad (17)$$

$$*OH + OH^- \rightarrow *O + H_2O + e^- \quad (18)$$

$$*O + OH^- \rightarrow *OOH + e^- \quad (19)$$

$$*OOH + OH^- \rightarrow O_2 + H_2O + e^- + * \quad (20)$$

The * are the active sites on the surface of an electrocatalyst. The combination of the two newly formed intermediates, *O, to quick produce O_2 gas is very difficult due to the large thermodynamic barrier [44]. OER is more complex than HER due to two H_2O molecules and four-electron oxidation processes to produce one O_2 molecule. OER takes place at the anode [45, 46]. OER needs the catalyst to be safe from the oxidation of O_2 and in aqueous media. Mostly transition metal nitrides are unstable throughout OER, especially in aqueous media. For the OER process, voltage is required higher than 1.23 V [47, 48].

1.5 Factors Affecting the Electrochemical Water Splitting Process

This section introduces the basic requirements for electrocatalysts. These are the turnover frequency (TOF), current density (j), Tafel slope, and overpotential (η). TOF is employed as performance indicators for electrocatalysts [49]. Both HER and OER half-reations, in practice, require a different potential to lower the kinetic barriers, and this additional potential is known as overpotential. At a given current density, overpotential deflects the catalytic activity. Lower the overpotential, the greater the electrocatalytic performance of

a catalyst. Tafel slope, a critical characteristic obtained from LSV, depicts the rising current rate as potential increases.

Another critical factor for determining the electrocatalytic activity of electrocatalysts is exchange current density (j_o), which is a crucial kinetic element in determining the reaction rate at equilibrium in electrochemical study. It indicates the rate at which an electrochemical reaction can take place when an electrocatalyst is used [50]. The Tafel slope is a significant measure of HER effectiveness since it is considered an inherent catalyst feature. By increasing voltage, a small Tafel slope suggests a faster rise in HER rate. An active site's TOF may be defined as the number of required product molecules with respect to time. The equation for TOF is [51],

$$\mathbf{TOF = j\ A/4nF} \qquad \mathbf{(21)}$$

Where A is the surface area of the active catalyst, n denotes the number of active sites, and F denotes the Faraday constant. Obtaining the accurate value of the TOF is difficult since it requires determining the correct number of active sites and ensuring that all catalyst sites are catalytically active. As a result, the TOF is an insufficient criterion for catalytic activity [52, 53].

OWS activity is influenced by the loading amount of catalyst, the geometric structure, the intrinsic element characteristic, and the coordination environment. It is common knowledge that each element possesses unique chemical characteristics. When the atomic structures of a single metal atom vary, they can exhibit distinct properties [54, 55]. The arrangement of active sites in an electrocatalyst is determined by its geometric structure. A structure would be catalytically efficient if all active sites were visible and accessible [56].. Selectivity is one of the most desirable factors of an electrocatalyst, together with activity and stability, which make up the necessary trio of characteristics for an electrocatalyst with selectivity [57]. Since selectivity is one of the most important characteristics of an electrocatalyst, it is crucial to reveal the selectivity of catalysts screened for OER and HER electrocatalysis by their FE in addition to the other activity parameters previously mentioned [58]. In addition, one can add other activity parameters beyond the discussed activity parameters if they are valid and acceptable. Any activity parameter that will be proposed for an electrocatalyst must deal with any of the one or

more following necessary criteria: selectivity, activity, and stability [59]. As an emerging catalytic material, MoP provides fresh insights into the mechanics of electrochemical processes.

1.6 Problem Statement

The demand and use of energy are increasing day by day and the only source of energy in the past was the natural resources i.e., oil and natural gas but with time these resources are depleted so researchers find an alternative for it in the shape of hydrogen which is a clean and pollution free source of energy. Hydrogen can be produced through many techniques like catalytic water reforming from methane and water splitting technique. Water splitting is used to produce H_2 in the presence of a catalyst. At first noble metal like Pt was used as a catalyst for this purpose but as they are more expensive and going to be depleted therefore there is a need to synthesize such catalyst which enhance the kinetics of the reaction and is less costly. In this research MoP/RGO based hybrids will be used as a catalyst to produce hydrogen gas. The method of electrochemical water splitting will be used in this research which is the splitting of water through electrolysis

1.7 Research Objective

The research objective is as follow

- Synthesis and characterization of MoP/RGO hybrids
- Lowering the overpotential of prepared hybrids
- Application of hybrids for HER (hydrogen evolution reaction) to see catalytic performance

1.8 Scope of Study

As Pakistan is a developing country and it has lack of many resources in form of energy so hydrogen production will cover that deficiency of energy because we can use that hydrogen as a fuel and in electricity and many more.

- One of the best advantages is that hydrogen produced in this process is renewable and as water is used which is the most abundant in nature so there is no problem

of depletion of water. Moreover, the use of transition metals as a catalyst will reduce the use of precious noble metal and prevent it from depletion.

- Hydrogen produced in the process of water splitting has many applications like it can be used as a domestic fuel, it can be used in vehicles, it can also be used as a raw material for many chemicals like ammonia etc.

1.9 Chapter Summary

This thesis consists of 5 chapters. The acquaintance of each chapter is given in the following chapters.

- **Chapter 1** delivers vision of the subject, background and contemporary problems related to the work. It also clarifies the problem statement, research objectives and scope of the planned study.
- **Chapter 2** will sketch the literature review achieved to describe the previous work done on the synthesis of MoP/RGO, previous method technique, water splitting and its factors. It also includes review based to compare MoP/RGO based hybrids with different hybrid electrocatalysts.
- **Chapter 3** covers the methodology related to the synthesis of pure MoP, pure GO, and hybrids.
- **Chapter 4** elaborate the result and discussion. The analysis of XRD and SEM to describe the phase of crystal structures and morphology of the synthesized catalysts. The chapter also elaborate Electrochemical studies of the active catalysts and its stability.
- **Chapter 5** reviews all the findings and conclusions in the current study and provides the future recommendation for the related work

Chapter 2

Literature Review

2.1 Literature Review

Using transition-metal-based materials as non-noble-metal HER electrocatalysts has been widely investigated [60-63], including sulfides [64-67], carbides, nitrides [68-71], and phosphides [72]. Among these catalysts, TMPs have got extensive interest due to their high conductivity and inherent activity comparable to noble metals, which can be ascribed to the electronegative phosphorus drawing electrons from metal ion desorption of hydrogen. Across the latest years, TMPs have demonstrated improved HER performance, with stability and high activity. MoP is a renowned HDS catalyst [73]. Since both HER and HDS need a reversible combination of H_2 and catalyst, MoP may exhibit superior HER catalytic activity [22]. This article compared and investigated the characteristics of Mo, Mo_3P, and MoP catalysts. The results indicated that catalysts with a higher P content in MoP exhibited greater catalytic activity than those with a lesser quantity of P or an absence of P in Mo_3P and Mo, respectively. Although MoP exhibited strong HER catalytic activity in bulk, it may be enhanced further by showing more active sites via nanostructures. Using $(NH_4)_2HPO_4$ as the P source, Xing et al. effectively synthesized a densely linked MoP nanoparticle network with several exposed active sites [74].

Notably, high activity and the unique network structure of MoP enable it to function very well in acidic solutions, with low overpotentials of 200 and 125 mV at 100 and 10 mA/cm^2, respectively.[75]. MoP@PC had the strongest catalytic activity against HER in acidic electrolytes compared to these composites and bulk MoP. Particularly, the same morphologies of these composites revealed that MoP possessed the greatest intrinsic catalytic activity, and MoP@PC outperformed the bulk, suggesting that it included more exposed catalyst active sites. Apart from porous carbon formed from MOF, composites based on carbon compounds may also increase their dispersion and performance. Heterointerface engineering significantly influences managing the interfacial and surface characteristics of a catalyst. However, regulating the quality and amount of

heterointerfaces at the 2D adjacent nanoscale remains a critical but demanding issue. Transition-metal interstitial compounds (TMICs) are similar to Pt in their potential as catalytic materials (Pt) [76, 77]. TMICs can activate and trap protons, making them active against HER [78, 79]. Mo, a naturally occurring element, may react with P and nitrogen (N) to generate Mo-based TMICs [10, 80, 81]. Structure engineering is critical for constructing the active interface and increasing the number of active catalytic sites, resulting in increased HER activity [82-86]. 2D materials are interesting catalysts in this area due to good exposure to a more accessible surface and their distinctive structure [87-91]. For instance, the 2D molybdenum nitrite strongly acts against HER with a η_{10}=129 mV [92]. Additionally, creating pores can improve mass transfer, enhancing performance enhancement [93-95]. An earlier study has shown that the small-sized Mo_2N-Mo_2C heterojunction anchored on holey RGO has effective HER performance [96]. A densely linked network of MoP particles (50 nm) proved efficient against HER (η_{10}=125 mV) [74]. The particles constituting the sheet and the sheet itself are relatively large, limiting its effectiveness against HER. As a result, developing 2D porous Mo-based TMIC heterojunction nanosheets composed of tiny particles is critical for efficient catalysis [97].

Table 1: A summary of different catalysts in 1M KOH.

Catalyst	**Loading (ug/cm^2)**	**$\eta_{j=10mA/cm^2}$**	**Tafel slope (mV/dec)**
MoB [98]	2300	0.225	–
MoCx [68]	800	~0.151	59
Ni-Mo alloy/Ti foil [99]	1000	0.08	–
Mo_2C [100]	102	0.176	58
MoP [101]	100	0.19	–
MoP/RGO [102]	337	140	72
MoP-RGO [102]	420	0.15	66

2.2 MoP and its Hybrids Synthesis Methods

Synthesis is critical in the creation of catalysts. To vary the reaction restrictions, the catalysts' exact size and structural morphologies are varied [103-105]. Catalyst manufacturing depends heavily on the synthesis process. Catalyst size and structural morphologies can be modified by adjusting reaction restrictions [106].

2.2.1 MoP and its Heterostructure Synthesis Methods

Synthesis is critical in the creation of catalysts. To vary the reaction restrictions, the catalysts' exact size and structural morphologies are varied [103-105]. Catalyst manufacturing depends heavily on the synthesis process. Catalyst size and structural morphologies can be modified by adjusting reaction restrictions [106]. Due to the adjustable lattice plane and huge specific surface area, 2D layered nanomaterials with larger lateral diameters showed a strong potential for attaining a high concentration of visible, active sites [107-109]. But, the production of nano-electrocatalysts of MoP is affected by the uneven distribution of the Mo-based nano-precursors and unavoidable severe particle aggregation as a result of the reaction temperature (usually more than 600°C), which results in a scarcity of active electrochemical sites and poor electron transfer, resulting in degraded HER performance [110, 111]. As a result, various strategies are developed by researchers for suppressing MoP aggregation by the addition of new components or their combination with supporting components. Fanhao Kong et al. formed a novel catalyst constituted of an amorphous bimetallic nanoarray of nickel molybdenum phosphate supported on NF by a combination of vapor-solid phosphating and hydrothermal techniques. The $NiMoO_4$ sample was placed in the furnace's center for phosphating. 1 g $NaH_2PO_2H_2O$ powder was put upstream of the flowing N_2. After spontaneously cooling under the protection of N_2 flow to ambient temperature, the phosphating sample NiMoPOx was collected. It shows improved HER and prolonged OER activity in 1M KOH. Additionally, $Ni(OH)_2$ and metallic Ni nanoparticles produced in situ on the primary $NiMoPO_x$ surface via OER and HER behave as electrocatalysts, significantly improving the performance of catalytic activity for OWS [112].

Table 2: Summary of electrochemical parameters determined for Pure MoP and single doped materials in 0.5M H_2SO_4 [113].

Catalyst	**Tafel slope (mV/dec)**	**TOF $(s^{-1})^2$**	**j_o (mA/cm^2)**	**C_{dl} (mF/cm^2)[3]**	**η_{10} (mV)**
MoP	87	0.12	0.51	53	115
Fe5-MoP	70	0.24	0.53	55	89
MoPS-3	71	0.15	0.52	76	92
Mn5-MoP	68	0.21	0.55	58	88
MoPS-1.5	70	0.18	0.55	65	89

2.2.2 MoP with RGO and CNT synthesis methods

Zexing Wu et al. proposed a technique for synthesizing MoP on graphene (MoP-RGO). MoP supported on graphene (MoP-RGO) was manufactured using a simple solvothermal method followed by phosphating at a high temperature. The material performs well in both alkaline and acid media. RGO prevents the nanoparticles from aggregating and facilitating electron transmission throughout the electrocatalytic process.

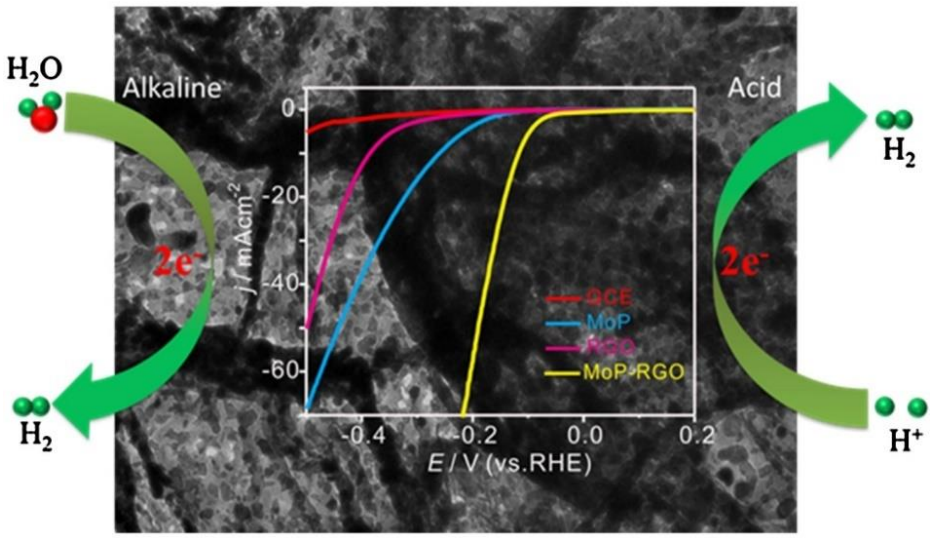

Figure 2: Graphical abstract of MoP-RGO synthesis [114].

Using a modified Hummer's method, GO can be synthesized by chemically oxidizing graphite. The synthesis of MoP-RGO is a two-step process. To begin, MoO_2-RGO was synthesized using the solvothermal technique. In ethylene glycol (EG), 120 mg of GO dispersed using sonication of $(NH_4)_6Mo_7O_{24}.6H_2O$ was included to the mixture while stirring. The mixture is heated at 200^{o}C for 10 h to make the black products. The black products were centrifuged, washed multiple times with water and ethanol, and freeze-dried. Then, the mixture is annealed for 2h at various temperatures in an H_2/Ar environment. Electrochemical measurements reveal that the nanocomposite of MoP-RGO produced at 900^{o}C has promising electrocatalytic activity for HER, at a j=10 mA/cm^2 with overpotentials of 150 mV and 117 mV in alkaline and acid environments, respectively.

Table 3: Electrochemical parameters for MoP/RGO based electrocatalysts [114].

	700^{o}C	800^{o}C	900^{o}C	1000^{o}C	MoP
Tafel slope (mV/dec)	**150**	**70**	**62**	**76**	**82**
j_0 (mA/cm^2)	**0.013**	**0.027**	**0.042**	**0.017**	**0.015**
Charge transfer impedance (V)	**730**	**34.5**	**24**	**445**	**545**
h (mV) j = 10 mA/cm^2	**400**	**200**	**117**	**231**	**260**

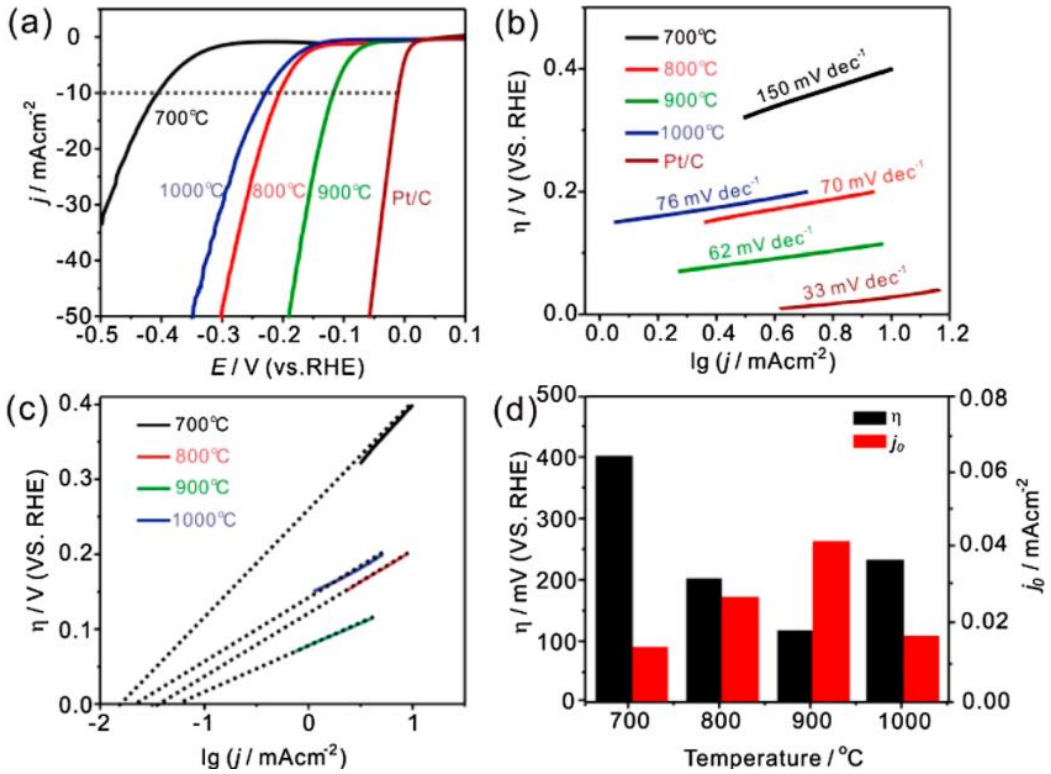

Figure 3: (a) Polarization curves obtained in 0.5M H_2SO_4 solution at a scan rate of 5 mV/s Tafel slopes (b) and j_o (c) of MoP-RGO (d) overpotentials and j_o of MoP [114].

Additionally, the catalyst's instability in the basic media was examined systematically. This study demonstrates an easy technique for simply producing a valuable carbon-supported metal phosphide electrocatalyst for HER [114]. Due to the incomplete production of MoP, the material displays the lowest electrocatalytic activity for the HER following heat treatment at 700°C. The materials' HER performance significantly increased at 800°C, particularly at 900°C, at 20 mA/cm^2 (η_{20}) with an overpotential of 142 and 117 mV at j= 10 mA/cm^2. Tafel slope determines polarization curves to ascertain the kinetics of HER (Fig. 3) [74, 115]. The NGR layers are responsible for the paper-like morphology evident in the Scanning Electron Microscopy (SEM) images (scale bar = 2 m). They are invisible due to the tiny size of the MoP particles. Normally, graphene layers are stacked on top of one another; however, in MoP/NCNTNGR, NCNTs are placed between the NGR layers, alleviating excessive NGR layer stacking and NCNT bundling [116].

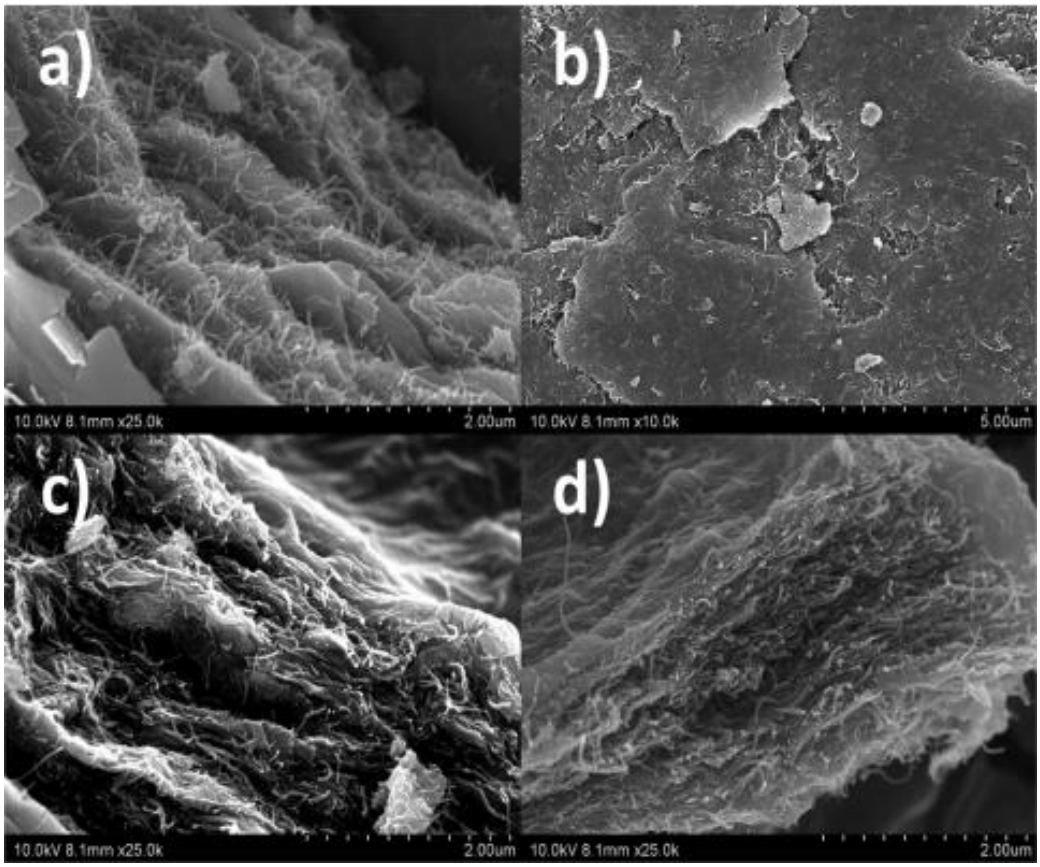

Figure 4: SEM micrographs of the MoP/NCNT-NGR sample indicate large-scale intercalation of NCNTs between NGR layers. The magnification was 25k [117].

Hui Xu et al. recently reported on successfully developing a modified form of hierarchical catalysts constituted of defect-rich nanosheets of Nickel-MoP (NiMoP). For efficient water splitting, nanosheets of NiMoP can be linked to the surface of CNTs. This study reports the synthesis of hierarchical NiMoP NSs@MCNTs using hydrothermal process. The findings were then analyzed by centrifuged and cleaned multiple times with acetone and ethanol. NiP NPs@MCNTs were synthesized using the same technique, except that $Na_2MoO_4.2H_2O$ was omitted. The schematic picture depicts the CNTs treated with 2-methylimidazole's capacity to bind Ni^{2+}, MoO_4^{2-}, and H_2PO^{2-} ions. After interacting with urea, these anchoring cations self-assembled on the surface of CNTs into conventional hierarchical nanosheets. Optimized Ni_1Mo_1P NSs@MCNTs require only 135 and 255 mV overpotentials, respectively, at a current of 10 mA/cm^2 for the OER and HER.

NSs@MCNTs/Ni_1Mo_1P. NSs@MCNTs couple to perform efficient water electrocatalysis at 10 mA/cm^2 and a relatively low overall potential of 1.601 V [118].

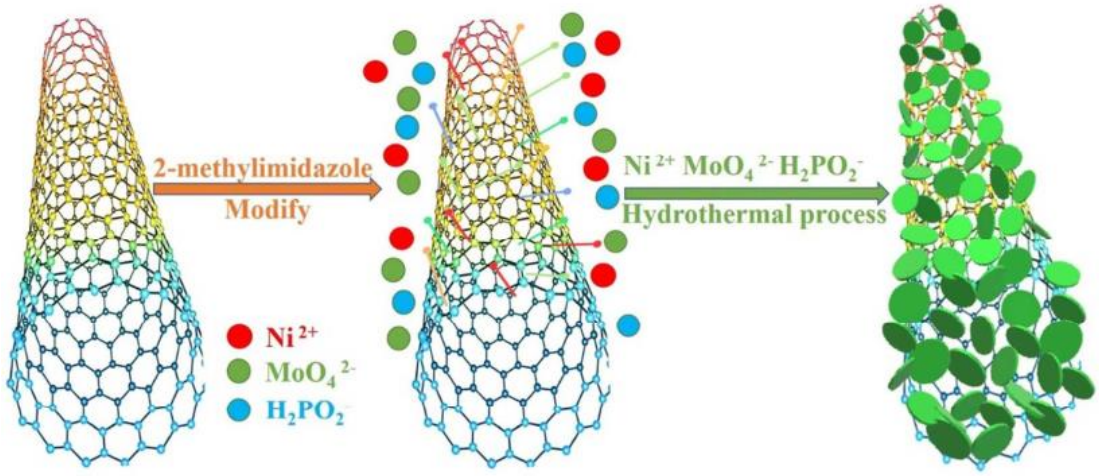

Figure 5: Preparation of NiMoP NSs@MCNTs [118].

2.2.3 MoP/MOF synthesis methods

Under high temperature and pressure conditions, hydrothermal preparation develops insoluble compounds from dissolved products in an aqueous solution. Hydrothermal preparation of MoP and its hybrids has been a low-cost and environment-friendly technology. While massive improvement has been made in electrochemistry, the search for high-level-efficiency catalysts for the concept of O_2 and H_2 by OWS remains a formidable task. Lifeng Lin demonstrated one-step method for fabricating new hierarchical MoP/NiFeP hollow spheres hybrid (MoP/NiFeP HSs) as bifunctional electrocatalysts. By doing 30min stirring, 100 L of NH_4OH is then added to start polymerization process, followed by dropwise applications of $Ni.(NO_3)_2$ solution (1 mg Ni $(NO_3)_2.6H_2O$ in 2 mL water). After 2 h of stirring, hollow spheres of Mo-PDA/NiFe-PBA-1 were collected centrifuged, washed with ethanol numerous times, and dried in an oven at 40°C. At room temperature cooling, the resultant black powder was deposited in the tube furnace with 1 g of $NaH_2PO_2H_2O$ and annealed for 2 h at 300°C with a ramp of 2°C/min under Ar and then for 1 h at 800°C with a ramping rate of 5°C/min to form MoP/NiFeP-1 HSs. The synthesis of MoP/NiFeP-2 HSs is like that of MoP/NiFeP-1 HSs,

except that Ni $(NO_3)_{26}H_2O$ and K_3. Fe $(CN)_6$ (4mg) are added in different proportions (4mg). Profiting from the highly interfacial coupling effects between NiFeP and MoP, hierarchical hollow structure, and the highly conductive graphitic carbon support, optimal MoP/NiFeP HSs exhibit effective catalytic performance in an alkaline electrolyte with very low overpotentials of 256 and 73 mV to achieve 100 and 10 mA/cm^2 for HER [119].

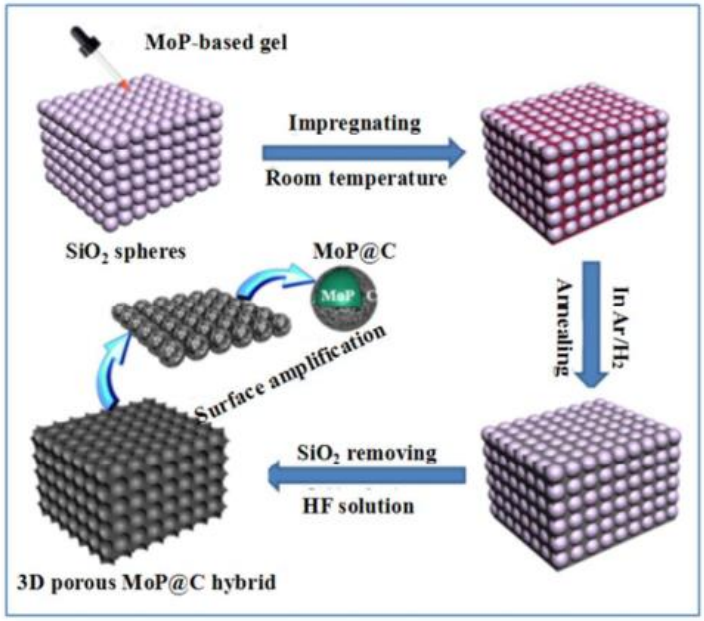

Figure 6: The 3D porous MoP@C hybrid synthesized method is shown schematically [120].

2.3 MoP and its Hybrids' Applications

Comparing HER and OER, OER during the OWS phase is rather sluggish kinetically and needs a large potential. Additionally, OER is extremely pH-dependent, operating differently in acidic and alkaline environments [1, 121]. In the primary medium, the hydroxyl radical group is shifted into O_2 and water at the expense of 1.230 V [122].

Linjie et al. synthesized nanohybrids of CQDs and MoP nanoparticles (CQDs/MoP) for the first time. CQDs considerably decrease surface oxidation and agglomeration of MoP nanoparticles to ensure that every MoP nanoparticle gets addressed electrically, enhancing MoP's intrinsic catalytic activity significantly. Investigating highly efficient nonnoble metal electrocatalysts for the HER in an alkaline environment is vital but still a substantial

challenge [123]. Xia et al. developed a unique 3D porous MoP@C hybrid that was employed for the 1st time only as an anode material for LIBs using a sol-gel process following annealing treatment. Following cycling, the resulting 3D porous MoP@C demonstrates long-term stability, better rate capability, and a high reversible capacity. The carbon layer's synergetic effect and 3D porous structure result in superior lithium storage capacity. By utilizing its structural and compositional advantages, the 3D porous MoP@C hybrid demonstrates improved lithium storage performance of specific capacity, cycling stability, and prolonged cycle life as an anode material for LIBs [120]. MoP was originally investigated as a catalyst for partial methane oxidation (POM) and compared to dry methane reforming (DRM). It was found that in POM and DRM processes, the dominant active site was MoP and that activity decreased. The MoP catalyst's redox mechanism proved critical for structural stability in methane reforming. The MoP catalyst has improved catalytic stability in POM compared to DRM, perhaps because of increased H_2 production in POM [124].

Table 4: Recent reported MoP/Hybrids-based electrocatalysts for overall electrocatalytic water splitting using 1M KOH electrolyte.

Electrocatalysts	**Type of reaction**	**Current density (mA/cm^2)**	**Overpotential (mV)**	**Tafel slope(mV/dec)**	**Stability(h)**	**Ref.**
Mo_2C-MoP/NPC	OER	10	320	44.77	168	[125]
Mo_2C-MoP/NPC	HER	10	120	50.31	168	[125]
MoP-Ru_2P/NPC	HER	10	47	36.93	12	[126]
MoP-Ru_2P/NPC	OER	10	260	70.89	12	[126]
MoP-Co@N,P-C	HER	10	152	76.8	24	[127]
MoP-Co@N,P-C	OER	10	296	97	24	[127]

MoP/SNG	HER	10	49	31.4	20	[128]
MoP/CNT	HER	10	86	73	40	[129]
(MoP)-CoP-$CoMoO_3$@CN	HER	10	198	95	10	[29]
(MoP)-CoP-$CoMoO_3$@CN	OER	10	296	105	10	[29]
Ce-Co (MoP)/MoP@C	O.E.R.	10	287	74.4	12(10% lose activity)	[130]
Ce-Co (MoP)/MoP@C	HER	10	188	72.2	12(10% lose activity)	[130]
MoP@NiFe-P hollow sphere	HER	10	73	31	40	[119]
MoP@NiFe-P hollow sphere	OER.	10	256	44	40	[119]
Ni-MoP@rGO	HER	10	122	71.4	-	[131]
Co-MoP@NCNNS-600	O.E.R.	10	270	60.3	105.6	[132]
Co-MoP@NCNNS-600	HER	10	62	38.1	105.6	[132]
MoP@rGO	HER	10	67	45	24	[133]
MoP-Ru_2P@NPC	HER	10	50	27.97	12	[134]
MoP@NC	HER	10	96	53	35	[135]
MoP NTs/Mo	HER	10	269	131.9	-	[136]

MoP@Ni_3P/NF	HER	10	45	56	30	[137]
MoP@Ni_3P/NF	OER.	35	331	50	35	[137]
MoP nanoflakes array	HER	10	114	54.6	20	[138]
MoP nanoflakes array	OER.	10	265	56.6	20	[138]
MoP/Ni_2P/NF	OER	35	330	77.6	12	[139]

Chapter 3

Materials and Methods

3.1 Chemicals and reagents

All the chemicals used to synthesize MoP hybrids with RGO were analytical grades. The chemicals that were used for MoP and GO involved Sodium Molybdate Dihydrate ($Na_2MoO_4 \cdot 2H_2O$), Sodium Hypophosphite Monohydrate ($NaH_2PO_2 \cdot H_2O$), Deionized water, Graphite powder, Sulfuric Acid (H_2SO_4), Sodium Nitrate ($NaNO_3$), Potassium Permanganate ($KMnO_4$), and Hydrogen Peroxide (H_2O_2) were procured from Sigma Aldrich.

3.2 Preparation of Pure Molybdenum Phosphide (MoP)

After mixing and grinding $Na_2MoO_4.2H_2O$ (300 mg) and $NaH_2PO_2.H_2O$ (3 g) in a mortar and pestle for 30 min, the uniformly grinded mixture was placed in a ceramic boat and calcined for 2 h at 750^oC (with a ramping rate of 10^oC/min) under an Ar atmosphere. Following the temperature drop, the obtained product was washed five times using deionized water to remove residues, then centrifugation was used to collect the final product, and dried overnight at 70^oC to produce the final product, Molybdenum Phosphide (MoP) [14].

3.3 Preparation of Pure Graphene Oxide (GO)

GO was synthesized using Hummers‘ method by graphite oxidation [140]. Graphite powder (2 g) was mixed with 46 mL of H_2SO_4, and 1 g of $NaNO_3$ was added while the temperature of the mixture was kept near 0°C using an ice bath. After stirring 2 h, $KMnO_4$ (6 g) was gradually added to the reaction mixture keeping the temperature at 20^oC. After adding the $KMnO_4$, remove the ice bath and keep the mixture at 35°C for 48 h. The mixture became pasty as the reaction progressed, and the colour turned from black to brownish grey. The heating was turned off, and deionized water (100 mL) was added dropwise to the mixture, causing it to rise to 98°C rapidly. After 15 min of stirring, the mixture was diluted with deionized water (200 mL). The colour was changed from brownish grey to

brown. The mixture was reduced by adding 10 mL of H_2O_2, and the reaction ended, resulting in a yellowish-brown colour. The mixture was left to settle overnight. The upper layer of graphene oxide (GO) was decanted after it settled in the beaker. The obtained product was centrifuged at 8000 rpm to remove the unreacted acid residues. Pure GO was obtained from centrifuge tubes after reaching pH 7, vacuum oven-dried overnight at 50°C.

3.4 Preparation of Hybrids of MoP with RGO

GO was added to a mixture of $Na_2MoO_4.2H_2O$ and $NaH_2PO_2.H_2O$, mixed and ground for 30 min in a mortar and pestle. The uniformly grinded mixture was placed in a ceramic boat and calcined for 2 h at 750^oC (with a ramping rate of 10^oC/min) under an Ar atmosphere. The GO in RGO decreased as heating increased. At high temperatures, oxygen-containing groups on GO sheets quickly burn into gases such as CO, CO_2, and H_2O, resulting in a considerable increase in pressure between GO sheets. High pressure overcomes van der Waals forces, causing the space between sheets to rise. Not only does thermal reduction release oxygen-containing groups, but it also exfoliates GO sheets. However, due to the high temperature or long annealing time, this process requires a lot of energy. At high temperatures, GO is exceedingly unstable, but RGO is extremely resilient. Following the temperature drop, the obtained product was washed five times with deionized water to remove reactant residues, and then centrifugation was used to collect the final product, dried at 70^oC overnight, the product was MoP/RGO hybrid. A constant amount of MoP was mixed with different amounts of GO to create unique product compositions such as MoP/RGO (10 mg), MoP/RGO (15 mg), and MoP/RGO (20 mg).

3.5 Characterization and Electrochemical study

X-ray Diffraction (XRD) (STOE-SEIFERTX'PER PRO) was used to investigate the phase detection of the synthesized materials. Cu-K radiation was used for compositional analysis, and the angle 2θ values ranged from 5° to 85°. The morphology and elemental analysis of prepared catalysts were observed using Scanning Electron Microscopy (SEM) (JEOL-JSM-6490A) connected with Energy Dispersive X-ray (EDX) analysis. The ink was prepared of the produced catalysts to study the electrochemical properties of all electrocatalysts. Polyvinylidene fluoride (PVDF) (2.5 mg) and N-methyl-2-pyrrolidone

(NMP) (0.3-0.5 mL) were mixed and stirred for 1 h after adding an active catalyst (42 mg) and carbon black (5 mg). After 4 h of sonication, the prepared ink was deposited on both sides of nickel foam and dried overnight at 70^{o}C. An electrochemical study was carried out using a 3-electrode on Origalys Potentiostat (OGF05A). Pt wire and Ag/AgCl were employed as counter and reference electrodes, respectively, and active catalyst was used as the working electrode. The catalytic activity of three electrodes in 1 M KOH solution was examined at various scan rates. Conventional reversible hydrogen electrode (RHE) potential was determined to simplify the calculation using Eq. (1).

$$\mathbf{E_{(RHE)} = E_{(Ag/AgCl)} + (0.059*pH) + 0.1976} \qquad \mathbf{(1)}$$

Turnover frequency was calculated using Eq. (2).

TOF equation is represented as,

$$\mathbf{TOF = (j*A)/(\alpha*\mathit{f}*n)} \qquad \mathbf{(2)}$$

j= Current density, A= An electrode's surface, *f*= Faraday constant, α= no of transported electrons n= Moles of material coated on the electrode's surface.

Stability of the active catalyst was determined using chronopotentiometry studies. Electrochemical Impedance Spectroscopy (EIS) was performed using an alternating current and a voltage of 10 mV over a frequency range of 200 kHz to 100 mHz. Electrochemical active surface area (A_{ECSA}) can be calculated as,

$$\mathbf{A_{ECSA} = C_p/C_s} \qquad \mathbf{(3)}$$

Where Cp = Electrochemical capacitance, C_s = Specific capacitance (40 µF/cm^2).

$$\mathbf{C_p = A/(2*m*k)\ (V_2\text{-}V_1)} \qquad \mathbf{(4)}$$

C_p: Electrochemical capacitance (F/g)

A: Area under the curve of CV graph

m: Mass of catalyst loaded (g)

k: Scan rate (V/s)

(V_2-V_1): Potential Window (V)

Chapter 4

Results and Discussion

4.1 Phase and structural analysis of MoP and its hybrids

The crystallinity of the prepared samples was analyzed using XRD in which all the samples were highly crystalline (Fig. 7 (A)). The XRD spectra of pure MoP are shown in Fig. 7 (A (a)). The XRD pattern shows that the synthesized MoP has hexagonal geometry (JCPDS card No. 03-065-6487). The prominent peaks of hexagonal MoP can be seen at angles 2θ of 27.87º, 32.03º, 42.95º, and 57.11º, which correspond to crystal faces (001), (100), (101), and (110), respectively. Pure MoP has a hexagonal structure like Pt-metal, indicating its potential as a non-Pt catalyst in the catalytic activity. XRD pattern of pure GO is shown in Fig. 7 (A (f)) and corresponds to the reported literature (JCPDS card No. 892482). The formation of GO was confirmed by a sharp diffraction peak with a d-spacing of 0.841 nm at angles 2θ of 10.95°, corresponding to the lattice plane (001). The presence of unexfoliated graphite results in a less intense peak at angle 2θ of 43.6°, corresponding to the plane (101) with a d-spacing of 0.212 nm. Due to the presence of oxygen functionalities at the edges of graphene sheets, the interactions are overcome, resulting in greater interlayer spacing in GO. Fig. 7 (A (e)) depicts the XRD pattern of RGO. The broad diffraction peak at angle 2θ of 24.5° with a plane (002) and d-spacing of 0.326 nm is confirmed in the literature (JCPDS card No. 75-1621). The broadening of the peak indicates the formation of a few layers of thick RGO sheets. Unexfoliated graphite causes the diffraction peak (1 0 1) at a 2θ of 43.55° and 0.2 nm inter-layer spacing. XRD patterns of hybrid MoP/RGO (10 mg), MoP/RGO (15 mg), and MoP/RGO (20 mg) are shown in Fig. 7 (A (b), (c), and (d)). The planes (001), (100), (101), and (110) of MoP can be seen clearly from the four peaks for all the MoP/RGO-based hybrids at 27.87°, 32.03°, 42.95°, and 57.11°, respectively, showing that there was no alteration in the crystal structure after the RGO was added to the MoP surface [141]. All characteristic planes of RGO exist as sharp peaks in all three prepared hybrids. While doing enlarged analysis of XRD patterns

for MoP and MoP/RGO based hybrids as shown in Fig. 7 (B), it can be seen that the prominent peaks located at 43º gradually shift to reduced 2θ angles by increasing contents of GO particularly in MoP/RGO (20 mg) hybrid had higher contents of graphene comparing other hybrids, which can be related to the lattice expansion and describes as other reported of doped MoP [142]. Using Scherrer's equation, X-ray line enlargement was studied to analyze the average crystallite sizes of structured materials [143].

$$\mathbf{L = (k.\ \lambda)/(FWHM)(Cos\theta_B)} \qquad \mathbf{(4)}$$

L = Size of crystallite

k = 0.9 (Scherrer constant) = Shape factor

λ = 0.15406 (nm) = X-ray wavelength

θ_B = Bragg angle

FWHM = Full width at half max.

Table 5: Crystallite sizes of different electrocatalysts.

Catalysts	FWHM	Peak positions (2θ)	Crystallite sizes (nm)	Average Crystallite size (nm)
MoP	0.182,0.255,0.328,0.182	27.872,32.033,42.957,57.114	47,33.5,26.7,52	39.8
GO	0.728,0.255	10.95,43.609	11.1,34.6	22.85
RGO	0.874,0.218	24.5,43.55	9.4,40.7	25.05
MoP/RGO (10 mg)	0.328,0.291,0.291,0.255	27.914,32.081,43.063,57.113	25.6,29.2,30.2,36.6	30.4
MoP/RGO (15 mg)	0.218,0.328,0.328,0.364	27.93,32.02,43.005,57.11	39,25.8,26.7,25.4	29.225
MoP/RGO (20 mg)	0.301,0.301,0.301,0.234	25.841,30.024,40.914,57.095	27.9,28.2,29.1,40	31.3

The average crystallite size of MoP, GO, RGO, MoP/RGO (10 mg), MoP/RGO (15 mg), MoP/RGO (20 mg) is 398Å (39.8 nm), 228.5Å (22.85 nm), 250.5Å (25.05 nm), 304Å (30.4 nm), 292.25Å (29.225 nm) and 313Å (31.3 nm) respectively.

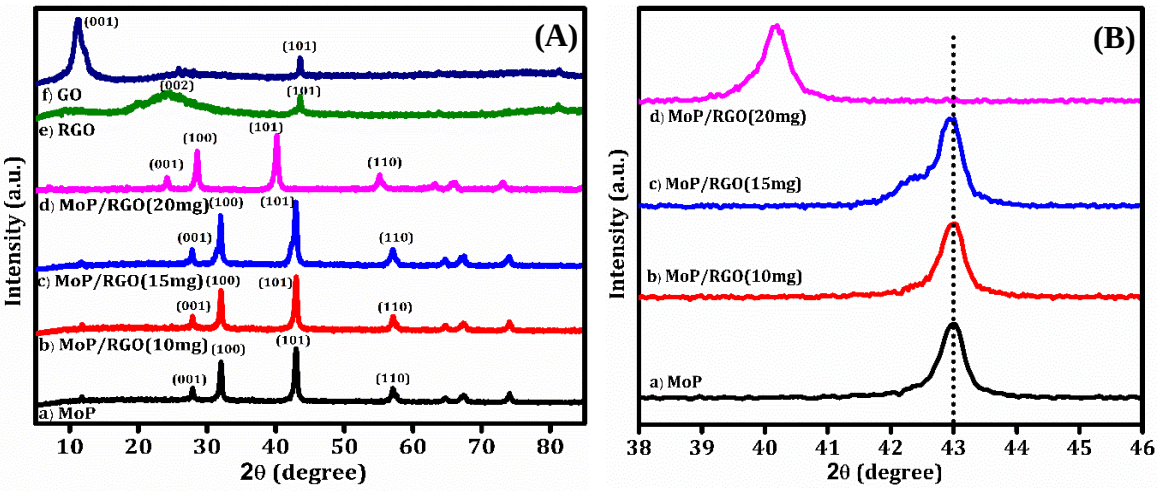

Figure 7: (A) XRD pattern of (a) MoP (b) MoP/RGO (10 mg) (c) MoP/RGO (15 mg) (d) MoP/RGO (20 mg) (e) RGO (f) GO (B) XRD enlargement section at peak (1 0 1) position of MoP and hybrids

The crystallinity of catalysts can be calculated using XRD data.

%Crystallinity = (A_C/A_C+A_a)*100 **(5)**

A_a: Amorphous peaks area, A_C: Crystalline peaks area

Table 6: Crystallinity of prepared catalysts using Origin.

Catalysts	**A_C**	**(A_C+A_a)**	**Crystallinity**
Pure MoP	1931.4016	2564	75.33%
MoP/RGO (10 mg)	1311.4557	2406.758	54.5%
MoP/RGO (15 mg)	732.725	1746.6291	63.42%
MoP/RGO (20 mg)	1402.6292	2545.92	55.1%

RGO	3353	4690.82	71.48%
GO	1798.93	4834.795	37.2%

4.2 Morphology and elemental analysis

The morphology of pure MoP and all hybrids was observed using SEM. As shown in Fig. 8 (a), there is agglomeration for MoP. It is shown that MoP is composed of small clusters of nanoparticles. The SEM images also show that highly porous interconnected MoP decorated on graphene oxide like sheet structure. The structural data of hybrids obtained from SEM scans reveal various structures and sizes, as shown in Fig. 8 (b, c, d), which is same as MoP/RGO reported. This porous nature increases the surface area and activity of these catalysts. The variation in the hybrid structure during calcination caused by the process causes a change in the quantity of GO. A rough surface was observed while synthesizing these hybrids having porous structure with clusters of nanoparticles in combination with GO. The presence of pores, which might be helpful in the spread of the gaseous molecules and electrolyte. These findings are matching with previous studies on the synthesis of MoP/RGO. According to the SEM images, the MoP/RGO has the same structure as the RGO [141, 144].

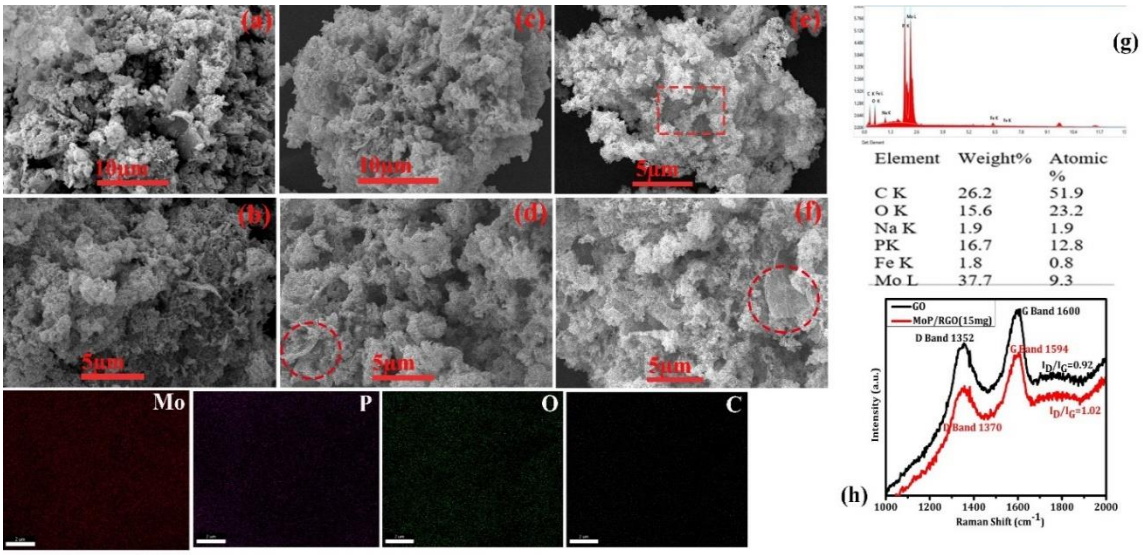

Figure 8: SEM image of **(a)** Low resolution Pure MoP **(b)** High resolution Pure MoP **(c)** Low resolution MoP/RGO (10 mg) **(d)** High resolution MoP/RGO (10 mg) **(e)** MoP/RGO (15 mg) **(f)** MoP/RGO (20 mg), EDS mapping of MoP/RGO (**Mo:** Molybdenum, **P:** Phosphorus, **O:** Oxygen, **C:** Carbon) **(g)** Subsequent elemental analysis spectrum of MoP/RGO (15 mg) hybrid **(h)** Raman spectrum of MoP/RGO (15 mg) and GO

EDX was used to ensure that the hybrid MoP/RGO (15 mg) contained all the necessary constituents. It demonstrates that hybrids are composed of elements such as Na, Mo, P, and C, with less oxygen presence from the partly oxidized MoP surface, as illustrated in Fig. 8 (g). The atomic percentages of Mo and P components are shown in Fig. 8 (g). The findings show that the hybrid's components are close together and evenly distributed. Because of the materials' superior recombination capabilities, the hybrid will exhibit superior charge separation and transfer capabilities, resulting in an even higher electrocatalytic performance. The EDS spectrum of MoP/RGO (15 mg) demonstrates that hybrids were successfully created. This spectrum shows the weight percentages of Mo, P, O, Na, and C. The GO and MoP/RGO (15 mg) Raman spectra were compared (Fig. 8 (h)). Peaks at 1370 and 1594 cm^{-1} for MoP/RGO (15 mg) correspond to the D and G carbon bands, respectively [145]. I_D/I_G ratio after MoP loading is caused by a solid interaction

between RGO and MoP, which causes an increase in RGO disorder. The Raman spectrum of GO is also shown in Fig. 8 (h). Raman spectra provide information about defects in graphitic material structures. GO displays two distinct bands. One band at 1352 cm^{-1} is referred to as the 'D band aroused' because of the disorder in the C=C aromatic system caused by oxygen functionalities and sp^3 hybridized carbon atoms. A second band at 1600 cm^{-1} is referred to as the Raman-allowed 'G band aroused' because of the C=C bond stretching of all the sp^2 hybridized carbon atoms. The relative ratio of the intensities of the D and G band (I_D/I_G) indicates structural disorders and defects [146]. I_D/I_G ratio in the case of GO is 0.92, confirming the oxidation of graphite.

4.3 Electrocatalytic Parameters

4.3.1 Hydrogen and Oxygen Evolution Reaction Kinetics

Electrochemical parameters of pure MoP and all three hybrids were measured in an alkaline solution of concentration 1 M KOH using a 3-electrode setup. HER activity of all electrocatalysts was measured using linear sweep voltammetry (LSV) curves, as shown in Fig. 9 (a). Significant improvement was observed of HER activity for hybrids than pure MoP. At current density (j)= 10 mA/cm^2, overpotentials of all hybrids, MoP/RGO (10 mg), MoP/RGO (15 mg), and MoP/RGO (20 mg), are required 161, 96, and 109 mV, respectively. The overpotentials of the standard Pt/C and Bare nickel foam are 75 and 295 mV, respectively, at j= 10 mA/cm^2. Best MoP/RGO (15 mg) hybrid has the lowest value compared to other hybrids, with an overpotential of 96 mV at j= 10 mA/cm^2. Because its electrical structure is like Pt-group metals, MoP is the most excellent TMP electrocatalyst for HER. It is also a highly active and stable electrocatalyst over a wide pH range [147]. Improving the conductivity or charge transfer ability of MoP-based electrocatalysts can be done by adding hybrid materials, such as RGO. The increased number of active sites in the hybrids (MoP/RGO) and compact heterojunctions between MoP and RGO can be attributed to the improved electrocatalytic H_2 molecule generation. The presence of more active edge sites on the MoP and RGO agglomeration could explain this increase—these sites slow charge carrier movement and recombination, resulting in improved electrocatalytic overall H_2 production.

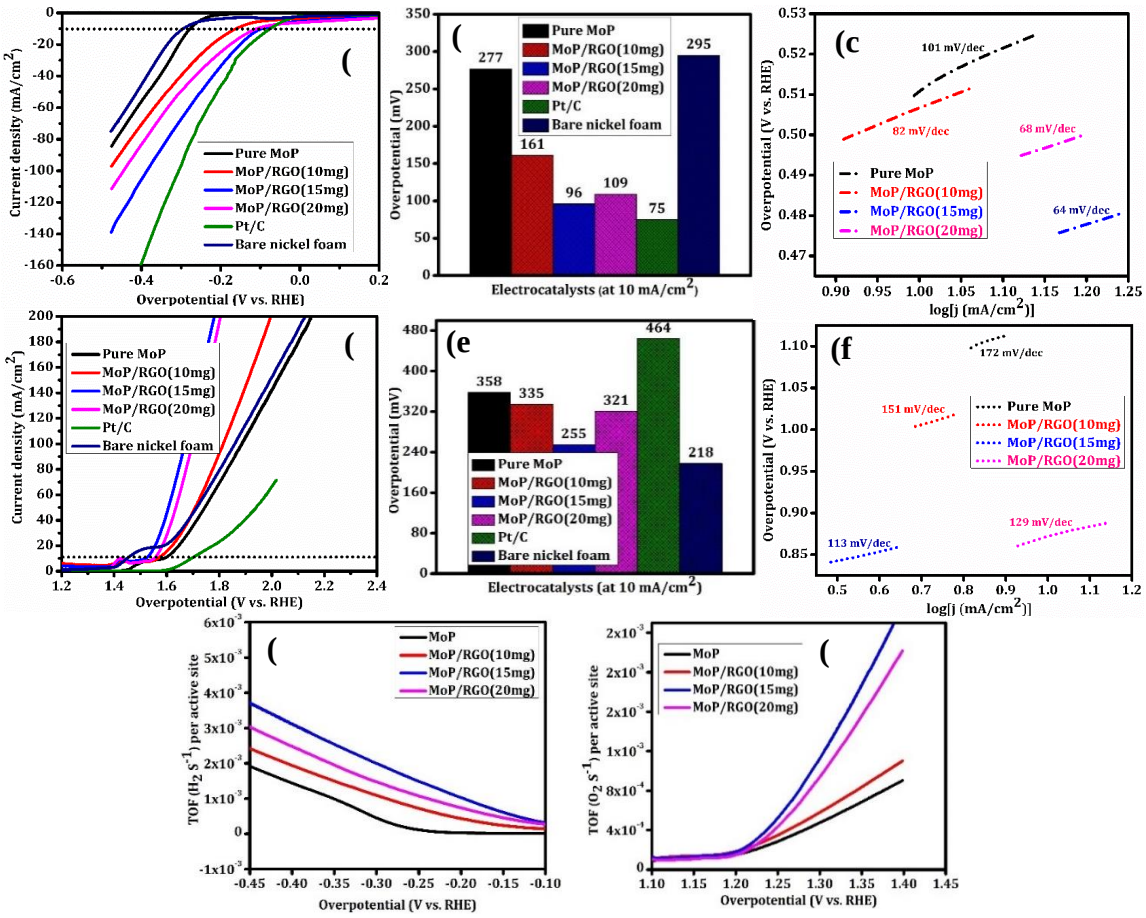

Figure 9: (a) LSV HER curves of Pure MoP, MoP/RGO (10mg, 15mg, 20mg), Pt/C, and Bare nickel foam (b) Overpotential required for HER (c) Corresponding TAFEL plots of Pure MoP, MoP/RGO (10mg, 15mg, 20mg) (d) LSV OER curves of Pure MoP, MoP/RGO (10mg, 15mg, 20mg), Pt/C, and Bare nickel foam (e) Overpotential required for OER (f) Corresponding TAFEL plots of Pure MoP, MoP/RGO (10mg, 15mg, 20mg) (g), (h) TOF curves

Furthermore, the conduction band potential of MoP is like that of RGO, resulting in faster electron mobility. The presence of more active edge sites promotes proton adsorption, which results in the formation of H_2 via reduction. Tafel values can be used to learn more about HER kinetics and catalytic performance of electrocatalysts using the Tafel equation [148].

$$\dot{\eta} = \dot{b} \log j + \alpha \qquad (5)$$

Here, ṅ, ƀ, and α represent the overpotential, Tafel slope, and Tafel constant, respectively. HER activities of the catalyst improve as the Tafel slope decrease. Tafel slope of MoP/RGO (15 mg) is around 64 mV/dec, which is less to the other catalysts used in this study, shown in Fig. 9 (c). Tafel slopes for pure MoP and MoP/RGO (10 mg and 20 mg) were 101, 82, and 68 mV/dec, respectively. Furthermore, the Tafel slope of the improved MoP hybrid is lower, indicating that MoP/RGO (15 mg) has different kinetics than the other electrocatalysts. The discharge of H_2O molecules in an alkaline solution on the catalyst surface results in a hydrogen adsorption intermediate. Previous research has shown that the increased surface area of MoP hybrids improves water dissociation, making them beneficial for HER in alkaline medium. The outstanding performance of RGO hybrids, such as MoP/RGO (15 mg), is due to a synergistic interaction between RGO and MoP, and the conductive support provided by nickel foam. As a result, H_2 adsorption increases, resulting in a more efficient electrocatalyst. By creating a limited route, nickel foam provides mechanical stability and facilitates ion passage into active sites. The excellent HER performance is due to the hexagonal structure of MoP based hybrids, which increases exposure to active sites. Furthermore, graphene can alter the electronic structure of Mo and P, resulting in improved HER performance. This Table 7 compares effective electrocatalysts for HER as reported in the literature.

Table 7: Different electrocatalysts for HER in 1M KOH solution.

Sr. No.	**Catalysts**	**Overpotential (mV)**	**j (mA/cm^2)**	**Tafel slope (mV/dec)**	**Stability (h)**	**Ref.**
1	**MoP/RGO (15 mg)**	**96**	**10**	**64**	**24**	**This work**
2	Mo_2C-MoP/NPC	120	10	50.31	168	[125]
3	MoP/CNT	86	10	73	40	[129]
4	Ce-Co (MoP)/MoP@C	188	10	72.2	12	[130]

5	Ni-MoP@rGO	122	10	71.4	-	[131]

To observe and analyze different catalytic kinetics, 4-electron transfer reaction mechanisms in alkaline media for OER was performed. OER activity of the produced electrocatalysts in an alkaline solution was studied using LSV curves (Fig. 9 (d)). These are evaluated using the anodic current densities, and overpotential of 1.6 V. MoP/RGO (15 mg) had the lowest overpotential of 255 and 327 mV at j= 10 mA/cm^2 and at j= 20 mA/cm^2, respectively. MoP/RGO (15 mg) required much less overpotential than pure MoP, MoP/RGO (10 mg), and MoP/RGO (20 mg), which are 358, 335, and 321 mV, respectively. Charge transfer is facilitated during electrochemical reactions due to the conductivity of MoP and graphene. The overpotentials of the standard Pt/C and Bare nickel foam are 464 and 218 mV, respectively, at j= 10 mA/cm^2. On the other hand, Pt/C has low OER activity due to the production of inactive surface oxide species [149].

The Tafel slopes for pure MoP and hybrids MoP/RGO (10 mg, 15 mg, and 20 mg) are 172, 151, 113, and 129 mV/dec, respectively, as shown in Fig. 9 (f). The Tafel value of MoP/RGO (15 mg) was lower than that of pure MoP, MoP/RGO (10 mg), and MoP/RGO (20 mg). MoP/RGO (15 mg) has better reaction kinetics and a faster oxygen evolution charge transfer capacity for OER. According to the findings, combining MoP and RGO in equal proportions is a more practical and effective strategy for improving catalytic performance. The low rate of hydroxyl ion adsorption on their surfaces is revealed by the pure MoP Tafel slope. When RGO is added, the OER kinetics are accelerated due to a smaller Tafel slope value. The smaller Tafel value indicates that the OER activity is acceptable to other commercial catalysts and thus significant. Low Tafel slope of MoP/RGO (15 mg) suggests that it is a 4-electron mechanism. As the potential increases, so does the rate of the catalyst, increasing electrocatalytic efficiency. The interaction of absorbed O_2 species with transition metal cation sites causes this remarkable occurrence. The heterostructure and interface of Mo, P and graphene particles promote electron transfer, resulting in superior electrochemical performance compared to individual Mo

and P particles. As shown in Fig. 9 (g), the turnover frequency (TOF) was also calculated to compare the intrinsic activities of produced catalysts. With increasing TOF values, RGO doping clearly improves the intrinsic activity of MoP catalysts. It should be noted that the MoP/RGO (15 mg) with the most possible RGO doping content had the highest TOF value, which may be attributed to the electronic structure optimization. In Table 8, different electrocatalysts for OER in 1M KOH solution are compared listed in the literature.

Table 8: Different electrocatalysts for OER in 1M KOH solution.

Sr. No.	**Catalysts**	**Overpotential (mV)**	**j (mA/cm^2)**	**Tafel slope (mV/dec)**	**Stability (h)**	**Ref.**
1	**MoP/RGO (15 mg)**	**255**	**10**	**113**	**24**	**This work**
2	MoP-Ru_2P/NPC	260	10	70.89	12	[126]
3	Co-MoP@NCNNS-600	270	10	60.3	105.6	[132]
4	Ce-Co (MoP)/MoP@C	287	10	74.4	12	[130]
5	MoP nanoflakes array	265	10	56.6	20	[138]

Cyclic voltammetry (CV) of MoP/RGO (15 mg) at different scan rates ranging from 5-100 mV/s of the applied voltage is shown in Fig. 10 (a). A pair of distinct redox peaks were detected in the potential range of 0-0.6 V. MoP/RGO (15 mg) layers transmit charge across redox sites, while ion transport due to electrode pores keeps the structure neutral. Basic process defines the reversibility of the adsorption of OH^{-1} at the electrode surface. CV profile remains constant as the scan rate increases, confirming the high cyclic stability of the catalyst, electrocatalytic efficiency and low resistance. Impedance of the absorber layer is reduced as the scan rate rises, resulting in a high current density. The number of

redox peaks gradually increases as the scan rate increases, showing that the redox activity is confined to the active sites of MoP/RGO (15 mg) and demonstrating the stability of a catalyst. Pure nickel foam does not provide within its potential range due to its low OER activity. It only serves as a conductive assist material [150]. Due to porous structure, nickel foam exhibits transmission channels and accelerates oxygen and hydrogen evolution. The loading Mo atom in the graphene-doped matrix, which has hexagonal structure, is responsible for the high electrocatalytic activity of MoP/RGO (15 mg). It prevents nanoparticles aggregation during catalytic reactions. Including an appropriate amount of Mo in the P matrix is also critical. Mo and P inclusion in the hexagonal structure of MoP progress electron transport. RGO increases activity by facilitating electron transfers and lowering charge transfer resistance.

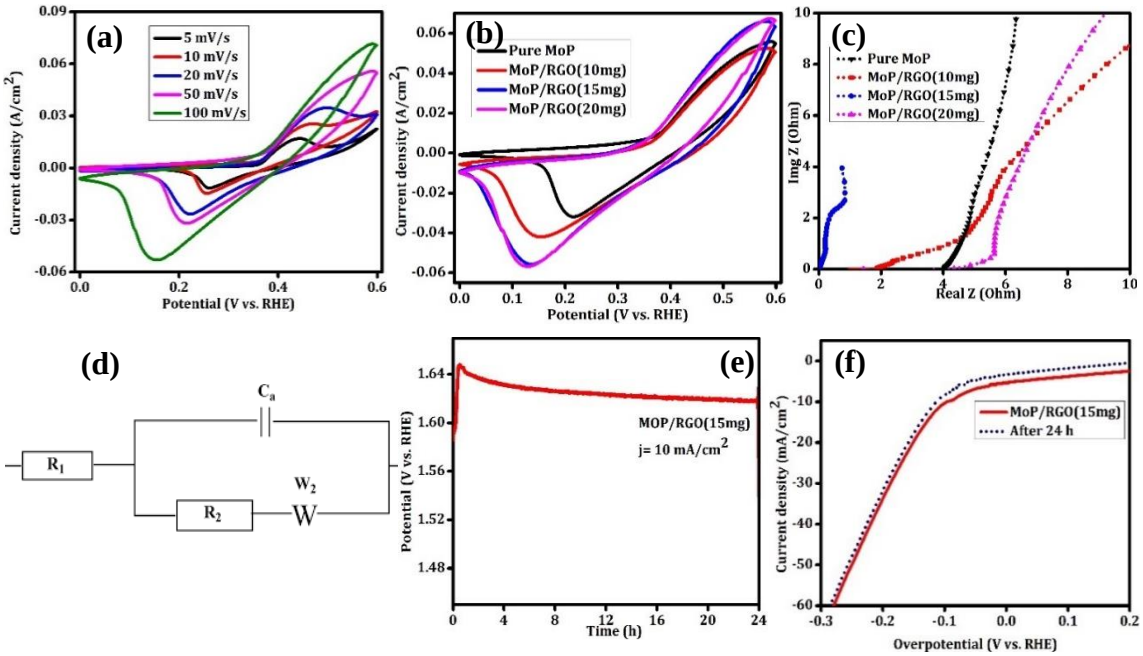

Figure 10: (a) Cyclic Voltammetry of MoP/RGO (15mg) at scan rates of 5-100 mV/s (b) Cyclic Voltammetry curves for Pure MoP, and hybrids (c) Nyquist plot at frequency 200 kHz-0.1 Hz of pure MoP, and MoP/RGO (10mg, 15mg, 20mg) (d) Fitting of the equivalent circuit from EIS-Nyquist plot (e) Chronopotentiometry to check the Stability of MoP/RGO (15mg) for 24 h (f) LSV HER curves before and after chronopotentiometry.

EIS was carried out to examine the performance of electrocatalysts at a frequency range of $2x10^5$ to 0.1 Hz as shown in Fig. 10 (c). R_1 and R_2 represent the ohmic and polarization resistances of the electrolytes between the electrodes. The Warburg impedance at the electrode-electrolyte contact is denoted by W, and the faradaic capacitance is denoted by C_a. As shown in Fig. 10 (c), MoP/RGO (15 mg) express a trend closer to the imaginary resistance on the y-axis, showing the electrocatalyst has a lower charge transport resistance. Similarly, it demonstrates that as the voltage of MoP/RGO (15 mg) increases, the charge transport resistance decreases significantly. In comparison, MoP/RGO (15 mg) has the least charge transfer resistance at the catalyst-electrolyte interface. The low R_{ct} of MoP/RGO (15 mg) suggests fast kinetics, which is consistent with the LSV results and values of TAFEL slopes. ECSA is a key measurement for analyzing the better electrocatalytic activity in the system and conducting additional research into the kinetics of the electrocatalysts. It is a critical approach for the electrochemical water-splitting

process. This method is frequently used to calculate non-faradic current at CV scan rates coupled to the $\dot{C}_{dl}$. This method calculates the $\dot{C}_{dl}$, and then used to calculate the ECSA of an electrocatalyst. However, because produced materials have sharp redox peaks, calculating non-faradic current using CV is more complicated. As a result, using EIS to calculate frequency-related impedance is an additional method for determining the $\dot{C}_{dl}$ value. Eq. (6) was used to calculate the $\dot{C}_{dl}$.

$$\dot{C}_{dl} = \frac{((Yo * R2)^{1/\alpha}}{R2} \quad (6)$$

$$ECSA = C_p/C_s \quad (7)$$

C_p: Electrochemical capacitance, C_s: Specific capacitance

McCrory reported a value of C_s (40 μF/cm^2) in an alkaline medium [151]. The constant phase element (CPE) method was used to calculate the equation parameters. Y_o is involved with the size of ability, whereas α is a dimensionless fit parameter relating to the deviation from the true capacitor. The MoP/RGO (15 mg) showed promising result when the value of $\dot{C}_{dl}$ was computed, which increased the electrolytic activity of the catalyst due to the precise ratio of Mo and P, improving the catalyst activity. The ECSA value of 3365 cm^2 for the MoP/RGO (15 mg) sample indicated a more significant number of active sites and better electron transport (Eq. 7). The occurrence of RGO may provide high electrical conductivity and improve ECSA of MoP. $\dot{C}_{dl}$ is linear proportional to the effective active sites of electrocatalysts, can be used to calculate the ECSA of the catalysts [152]. Also, the formation of MoP/RGO enhances electron transport and lowers the barrier of charge transfer, which increases catalytic activity.

Tabel 5: Comparative value of R_s, R_{ct} and ECSA

Catalysts	**R_s (ohm)**	**R_{ct} (ohm)**	**ECSA (cm^2)**
MoP	4.2	5.519	2104
MoP/RGO (10 mg)	1.02	4.053	2853

MoP/RGO (15 mg)	0.01	0.04	3365
MoP/RGO (20 mg)	0.08	1.453	3291

Stability is an important parameter for practical applications of electrocatalysts. Chronopotentiometry at an accelerated scanning rate was used to investigate the stability of the MoP/RGO in alkaline media. Furthermore, the durability of the catalyst is essential for the increasing application of the concept of H_2 production as a fuel. The stability (24 h) of MoP/RGO (15 mg) is shown in Fig. 10 (e). According to the chronopotentiometry data, the catalyst exhibited some unsteady behaviour, which may be attributed to its structural features. Following an immediate response, the potential remained unsteady for the first 5 h. Furthermore, H_2 production process at the cathode led to an initial rapid rise in cell potential. It is because the synthesized catalyst was activated during testing. The addition of a graphene layer improved the stability, limiting corrosion during HER activity of an electrocatalyst. The LSV curve changes slightly after 24 h of chronopotentiometry, indicating good stability of MoP/RGO (15 mg) in the HER activity. The MoP/RGO stability is due to the MoP particles being closely immobilized on the RGO support. It can be seen from comparing the LSV before and after the stability test that the catalyst retains stability and activity after 24 h (Fig. 10 f).

4.4 Proposed Mechanism

The Volmer-Heyrovsky reaction mechanism is proposed based on the reaction conditions and values of HER Tafel plots. It should be noted that in the Volmer reaction, the first step in alkaline pH involves proton abstraction from water. In the second step, hydrogen is generated by electrochemical desorption of hydrogen (Heyrovsky step). The reaction mechanism is shown in Eq. (9) and (10) (Fig. 11).

1. Volmer reaction:

$$\mathbf{H_2O + e^- \longrightarrow H^* + OH^-} \qquad \mathbf{(9)}$$

2. Heyrovsky reaction:

$$H_2O + e^- + H^* \longrightarrow H_2 + OH^- \quad (10)$$

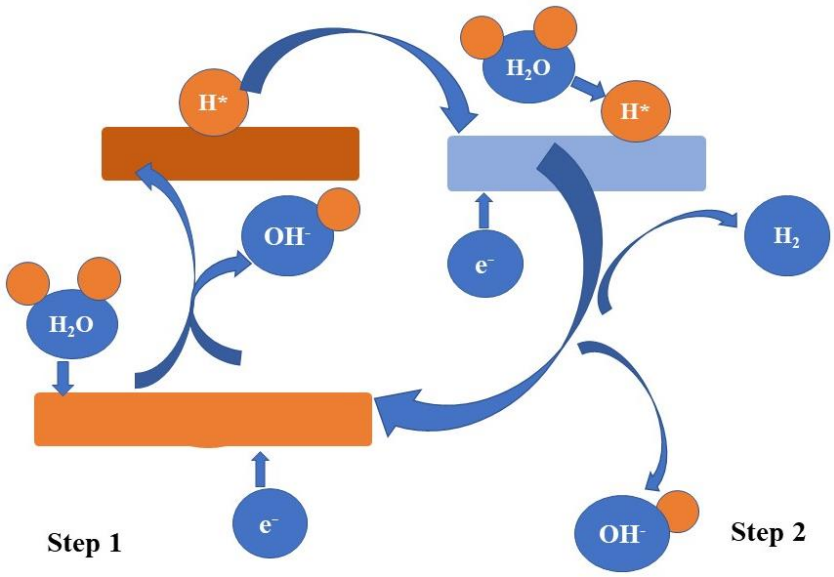

Figure 11: Proposed Schematics for HER on MoP/RGO (15 mg).

Oxidation process is a 4-step mechanism including multiple intermediates in the basic environment. The OER is represented in Eq. (11)– (14).

$$M + OH^- \longrightarrow MOH + e^- \quad (11)$$

$$MOH + OH^- \longrightarrow MO + H_2O + e^- \quad (12)$$

$$MO + OH^- \longrightarrow MOOH + e^- \quad (13)$$

$$MOOH + OH^- \longrightarrow M + O_2 + H_2O + e^- \quad (14)$$

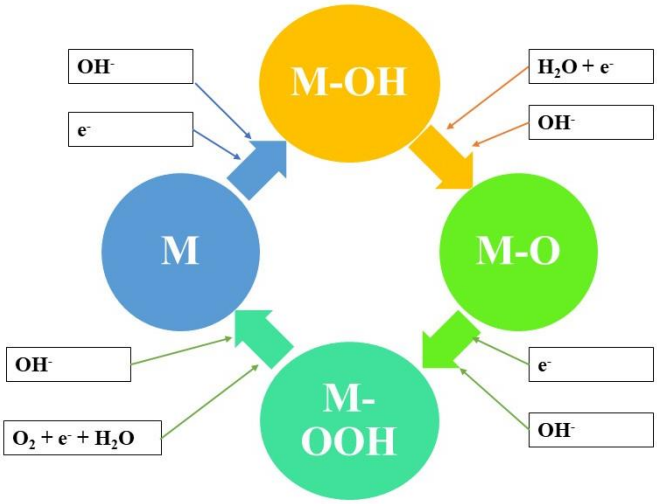

Figure 12: Proposed Schematics for OER on MoP/RGO (15 mg).

Conclusions

This research details MoP-based electrocatalysts on RGO substrates for the HER in alkaline medium. We are especially interested in improving electrochemical performance and methods for increasing HER activity. The improved MoP/RGO electrocatalyst exhibits excellent performance for HER in an alkaline solution, with an overpotential of 96 mV and a Tafel slope of 64 mV/dec at j=10 mA/cm^2. By using rational RGO as support for MoP-based electrocatalysts, it is possible to modify the properties of MoP-based HER catalysts. Furthermore, this method applies to most known Mo-based electrocatalysts, including Mo_xC, MoS_x, $MoSe_x$, and other MoP-containing electrocatalysts. The exceptional performance is attributed to the addition of RGO in MoP-based hybrids resulting in (1) clumping pervention of pure MoP-based electrocatalysts; (2) increasing electronic conductivity; (3) easing the diffusion of the electrolyte and the gas produced; and (4) improving the catalysts' long-term durability. Such findings offer a new avenue for the rational design of RGO substrate hybrid catalysts for improved water-splitting applications. Due to its greater HER catalytic activity and stability across a wide pH range, MoP-based materials are the most desirable candidates for replacing the costly but common Pt-based catalysts. Due to its low overpotential, porosity, stability, inexpensive and abundant nature, compatibility, and permeability, MoP is exceptional and ideal for electrocatalytic applications and processes.. Presently, considerable research efforts have enabled all Mo-based electrocatalysts to exhibit good HER performance in acidic electrolytes. An ideal catalyst should possess sufficient hydrogen adsorption energy, enough active sites, and suitable electrical conductivity.

Recommendation

Despite rapid advancements in using MoP-based materials as HER catalysts, few crucial and problematic challenges remain. MoP's electrical conductivity through electrochemical H_2 production is a critical factor to consider. Because P atoms have high electronegativity, they significantly inhibit the delocalization of electrons of metal atoms, resulting in decreased conductivity. As the P concentration rises, the TMPs' conductivity steadily declines, resulting in a semi-conductive or insulating property. Thus, the P content of MoP must be carefully studied and adjusted to improve HER activity and conductivity. Thorough knowledge of the catalytic activity of TMPs-based catalysts throughout the HER process is critical for developing improved electrocatalysts. It is critical to examine how catalysts evolve structurally and how reactants, intermediates, and products are converted. Ex-situ approaches could fail to examine the rebuilt surface and offer actual evidence about the intermediate's development due to the fleeting states and unavoidable air oxidation of catalysts and unstable intermediate species. As a result, in-situ characterization methods such as in-situ X-ray absorption spectroscopy and in-situ Raman are commonly employed while operating a basic system of electrochemical processes. Such in situ research explains active natural centers and reaction mechanisms and helps to develop improved electrocatalysts. DFT theoretical simulations have become a progressively viable method for predicting performance and designing catalysts. In the case of TMP-based catalysts as HER-active, DFT simulations can reveal the modified interaction and electronic structure of reactive species with the structure surface and the development of intermediates.

Additionally, theoretical computations may forecast the best crystal shapes and chemical constitutions. However, numerous unanswered questions remain. For example, realistic models which closely resemble real-world reaction systems are critical for DFT theoretical computations. It is critical to comprehend the MoP-driven HER process to simulate electrocatalysts and reaction routes accurately. When considering large-scale applications of MoP-based HER electrocatalysts, three major factors must be considered: catalytic activity, durability, and commercial availability. While MoP-based materials have been

described as potential electrocatalysts for HER, their activity must be increased further compared to the Pt/C state-of-the-art catalyst. Durability is also a critical yet difficult problem for electrocatalysts based on MoP. Hydrogen adsorption energy, conductivity, nanostructure, and super oleophobic surface must be developed logically and regulated precisely. These key features interact with one another and independently fulfill distinct tasks, optimizing the performance of MoP-based catalysts. Additionally, Fe and Ni-based phosphides are regarded as potential long-term HER electrocatalysts due to their abundance on Earth. Apart from the availability of materials, practical applications require cost-effective and energy-efficient synthesiz techniques.

References

1. Jiao, Y., et al., *Design of electrocatalysts for oxygen-and hydrogen-involving energy conversion reactions.* 2015. **44**(8): p. 2060-2086.
2. Ali, M., et al., *Recent advancements in MOF-based catalysts for applications in electrochemical and photoelectrochemical water splitting: A review*. 2021. **45**(2): p. 1190-1226.
3. Zheng, Y., Y. Jiao, and S.Z.J.A.M. Qiao, *Engineering of carbon-based electrocatalysts for emerging energy conversion: from fundamentality to functionality*. 2015. **27**(36): p. 5372-5378.
4. Rabi, O., et al., *An inclusive review on the synthesis of molybdenum carbide and its hybrids as catalyst for electrochemical water splitting.* 2020. **494**: p. 111116.
5. Abdullah, U., et al., *An inclusive perspective on the recent development of tungsten-based catalysts for overall water-splitting: A review.* 2022.
6. Hu, Q., et al., *Recent progress in the hybrids of transition metals/carbon for electrochemical water splitting.* 2019. **7**(24): p. 14380-14390.
7. Wu, C., et al., *Molybdenum carbide-decorated metallic cobalt@ nitrogen-doped carbon polyhedrons for enhanced electrocatalytic hydrogen evolution.* 2018. **14**(16): p. 1704227.
8. Xiong, B., L. Chen, and J.J.A.C. Shi, *Anion-containing noble-metal-free bifunctional electrocatalysts for overall water splitting.* 2018. **8**(4): p. 3688-3707.
9. Zhao, H., Z.-Y.J.C.S. Yuan, and Technology, *Transition metal–phosphorus-based materials for electrocatalytic energy conversion reactions.* 2017. **7**(2): p. 330-347.
10. Shi, Y. and B.J.C.S.R. Zhang, *Recent advances in transition metal phosphide nanomaterials: synthesis and applications in hydrogen evolution reaction.* 2016. **45**(6): p. 1529-1541.
11. Du, H., et al., *Recent progress in transition metal phosphides with enhanced electrocatalysis for hydrogen evolution.* 2018. **10**(46): p. 21617-21624.

12. Zahra, R., et al., *Three-dimensional hierarchical flowers-like cobalt-nickel sulfide constructed on graphitic carbon nitride: Bifunctional non-noble electrocatalyst for overall water splitting.* 2022. **418**: p. 140346.
13. Rabi, O., et al., *Bifunctional molybdenum carbide based hybrids for electrocatalytic water splitting.* 2021. **47**(17): p. 24949-24958.
14. Cheng, C., et al., *Facile preparation of nanosized MoP as cocatalyst coupled with g-C3N4 by surface bonding state for enhanced photocatalytic hydrogen production.* 2020. **265**: p. 118620.
15. Zhou, X., et al., *Design and epitaxial growth of MoSe2–NiSe vertical heteronanostructures with electronic modulation for enhanced hydrogen evolution reaction.* 2016. **28**(6): p. 1838-1846.
16. Song, J., et al., *Bimetallic cobalt-based phosphide zeolitic imidazolate framework: CoPx phase-dependent electrical conductivity and hydrogen atom adsorption energy for efficient overall water splitting.* 2017. **7**(2): p. 1601555.
17. Ehsan, M.A., A.S. Hakeem, and A.J.S.r. Rehman, *Synergistic effects in bimetallic Pd–CoO electrocatalytic thin films for oxygen evolution reaction.* 2020. **10**(1): p. 1-11.
18. Wang, F., et al., *Interface engineered WxC@ WS2 nanostructure for enhanced hydrogen evolution catalysis.* 2017. **27**(7): p. 1605802.
19. Wang, P., et al., *Precise tuning in platinum-nickel/nickel sulfide interface nanowires for synergistic hydrogen evolution catalysis.* 2017. **8**(1): p. 1-9.
20. Kuang, P., et al., *In situ fabrication of Ni–Mo bimetal sulfide hybrid as an efficient electrocatalyst for hydrogen evolution over a wide pH range.* 2017. **7**(9): p. 6179-6187.
21. Wang, X.-D., et al., *Novel porous molybdenum tungsten phosphide hybrid nanosheets on carbon cloth for efficient hydrogen evolution.* 2016. **9**(4): p. 1468-1475.
22. Xiao, P., et al., *Molybdenum phosphide as an efficient electrocatalyst for the hydrogen evolution reaction.* 2014. **7**(8): p. 2624-2629.

23. Yue, Q., et al., *MoP is a novel, noble-metal-free cocatalyst for enhanced photocatalytic hydrogen production from water under visible light.* 2015. **3**(33): p. 16941-16947.
24. Yin, Y., et al., *MoP hollow nanospheres encapsulated in 3D reduced graphene oxide networks as high rate and ultralong cycle performance anodes for sodium-ion batteries.* 2019. **11**(15): p. 7129-7134.
25. Ge, R., et al., *Hierarchical molybdenum phosphide coupled with carbon as a whole pH-range electrocatalyst for hydrogen evolution reaction.* 2020. **260**: p. 118196.
26. Choi, S., et al., *Reduced graphene oxide-based materials for electrochemical energy conversion reactions.* 2019. **1**(1): p. 85-108.
27. Noor, T., et al., *Nanocomposites of NiO/CuO based MOF with rGO: An efficient and robust electrocatalyst for methanol oxidation reaction in DMFC.* 2020. **10**(8): p. 1601.
28. Khan, M.W., et al., *Nitrogen-Doped Oxygenated Molybdenum Phosphide as an Efficient Electrocatalyst for Hydrogen Evolution in Alkaline Media.* 2020. **8**: p. 733.
29. Yu, L., et al., *Cobalt/molybdenum phosphide and oxide heterostructures encapsulated in N-doped carbon nanocomposite for overall water splitting in alkaline media.* 2019. **11**(7): p. 6890-6899.
30. Luo, S. and P.K.J.A.n. Shen, *Concave platinum–copper octopod nanoframes bounded with multiple high-index facets for efficient electrooxidation catalysis.* 2017. **11**(12): p. 11946-11953.
31. Han, L., S. Dong, and E.J.A.m. Wang, *Transition-metal (Co, Ni, and Fe)-based electrocatalysts for the water oxidation reaction.* 2016. **28**(42): p. 9266-9291.
32. Song, J., et al., *A review on fundamentals for designing oxygen evolution electrocatalysts.* 2020. **49**(7): p. 2196-2214.
33. Tian, Y., et al., *Metal-Organic Frameworks Derived Multidimensional CoP/N, P-Doped Carbon Architecture as an Efficient Electrocatalyst for Overall Water Splitting.* 2021. **13**(13): p. 3037-3045.

34. Browne, M.P., et al., *Layered and two dimensional metal oxides for electrochemical energy conversion.* 2019. **12**(1): p. 41-58.
35. Abdullah, U., M. Ali, and E. Pervaiz, *An Inclusive Review on Recent Advancements of Cadmium Sulfide Nanostructures and its Hybrids for Photocatalytic and Electrocatalytic Applications.* Molecular Catalysis, 2021. **508**: p. 111575.
36. Xie, J., et al., *Atomically-thin molybdenum nitride nanosheets with exposed active surface sites for efficient hydrogen evolution.* 2014. **5**(12): p. 4615-4620.
37. Michalsky, R., Y.-J. Zhang, and A.A.J.A.C. Peterson, *Trends in the hydrogen evolution activity of metal carbide catalysts.* 2014. **4**(5): p. 1274-1278.
38. Kou, Z., et al., *A sacrificial Zn strategy enables anchoring of metal single atoms on the exposed surface of holey 2D molybdenum carbide nanosheets for efficient electrocatalysis.* 2020. **8**(6): p. 3071-3082.
39. Hughes, J., et al., *Polymer electrolyte electrolysis: A review of the activity and stability of non-precious metal hydrogen evolution reaction and oxygen evolution reaction catalysts.* 2021. **139**: p. 110709.
40. Ďurovič, M., J. Hnát, and K.J.J.o.P.S. Bouzek, *Electrocatalysts for the hydrogen evolution reaction in alkaline and neutral media. A comparative review.* 2021. **493**: p. 229708.
41. Zhang, K., et al., *Molybdenum selenide electrocatalysts for electrochemical hydrogen evolution reaction.* 2019. **6**(14): p. 3530-3548.
42. Zhang, B., et al., *Improving hydrogen evolution reaction performance by combining ditungsten carbide and nitrogen-doped graphene: A first-principles study.* 2021. **172**: p. 122-131.
43. Li, W.-Z., et al., *The electronic properties and catalytic activity of precious-metals adsorbed silicene for hydrogen evolution reaction and oxygen evolution reaction.* 2021. **560**: p. 150041.
44. Rossmeisl, J., et al., *J. Electroanal. Chem.* 2007.

45. Zhang, H., et al., *Unveiling the activity origin of electrocatalytic oxygen evolution over isolated Ni atoms supported on a N-doped carbon matrix.* 2019. **31**(48): p. 1904548.
46. Liang, S., et al., *Nickel–Iron Nitride–Nickel Sulfide Composites for Oxygen Evolution Electrocatalysis.* 2020. **12**(37): p. 41464-41470.
47. Skúlason, E., et al., *Modeling the electrochemical hydrogen oxidation and evolution reactions on the basis of density functional theory calculations.* 2010. **114**(42): p. 18182-18197.
48. Tareen, A.K., et al., *Nickel-based transition metal nitride electrocatalysts for the oxygen evolution reaction.* 2019. **12**(17): p. 3941-3954.
49. Nørskov, J.K., et al., *Origin of the overpotential for oxygen reduction at a fuel-cell cathode.* 2004. **108**(46): p. 17886-17892.
50. Yan, Y., et al., *Recent development of molybdenum sulfides as advanced electrocatalysts for hydrogen evolution reaction.* 2014. **4**(6): p. 1693-1705.
51. Mazzucato, M., et al., *Effects of the induced Micro-and Meso-porosity on the single site density and turn over frequency of Fe-NC carbon electrodes for the Oxygen Reduction Reaction.* 2021. **291**: p. 120068.
52. Bhadra, B.N., et al., *Oxidative denitrogenation of liquid fuel over W2N@ carbon catalyst derived from a phosphotungstinic acid encapsulated metal–azolate framework.* 2021. **285**: p. 119842.
53. Shen, H., et al., *Supporting Nickel on Vanadium Nitride for Platinum Comparable Hydrogen Evolution in Alkaline Solution.* 2021.
54. Zhong, W., et al., *C 2 N-supported single metal ion catalysts for HCOOH dehydrogenation.* 2018. **6**(24): p. 11105-11112.
55. Wang, Y., X. Huang, and Z.J.C.J.o.C. Wei, *Recent developments in the use of single-atom catalysts for water splitting.* 2021. **42**(8): p. 1269-1286.
56. Deng, C., et al., *A single-atom catalyst of cobalt supported on a defective two-dimensional boron nitride material as a promising electrocatalyst for the oxygen reduction reaction: a DFT study.* 2019. **21**(13): p. 6900-6907.

57. Anantharaj, S., K. Karthick, and S.J.M.T.E. Kundu, *Evolution of layered double hydroxides (LDH) as high performance water oxidation electrocatalysts: A review with insights on structure, activity and mechanism.* 2017. **6**: p. 1-26.
58. Anantharaj, S., et al., *6, 8069–8097; b) L. Han, S. Dong, E. Wang.* 2016. **28**: p. 9266-9291.
59. Fabbri, E., et al., *Catal Sci Technol 4: 3800–3821 https://doi. org/10.1039*. 2014, C4CY00669K.
60. Gong, M., et al., *Nanoscale nickel oxide/nickel heterostructures for active hydrogen evolution electrocatalysis.* 2014. **5**(1): p. 1-6.
61. Xu, Y.F., et al., *Nickel/nickel (II) oxide nanoparticles anchored onto cobalt (IV) diselenide nanobelts for the electrochemical production of hydrogen.* 2013. **125**(33): p. 8708-8712.
62. Jiang, A., et al., *Ionic liquid-assisted synthesis of hierarchical one-dimensional MoP/NPC for high-performance supercapacitor and electrocatalysis.* 2020. **8**(16): p. 6343-6351.
63. Chen, B., et al., *Ex-situ flame co-doping of tin and tungsten ions in TiO2 nanorod arrays for synergistic promotion of solar water splitting.* 2020. **226**: p. 115843.
64. Hu, J., et al., *Hydrogen evolution electrocatalysis with binary-nonmetal transition metal compounds.* 2017. **5**(13): p. 5995-6012.
65. Zhang, X., et al., *Solution-processed two-dimensional MoS2 nanosheets: preparation, hybridization, and applications.* 2016. **55**(31): p. 8816-8838.
66. Voiry, D., et al., *Enhanced catalytic activity in strained chemically exfoliated WS2 nanosheets for hydrogen evolution.* 2013. **12**(9): p. 850-855.
67. Gong, G., et al., *Ag doping of Zn-In-S quantum dots for photocatalytic hydrogen evolution: Simultaneous bandgap narrowing and carrier lifetime elongation.* 2017. **216**: p. 11-19.
68. Wu, H.B., et al., *Porous molybdenum carbide nano-octahedrons synthesized via confined carburization in metal-organic frameworks for efficient hydrogen production.* 2015. **6**(1): p. 1-8.

69. Zhu, J., et al., *A general salt-templating method to fabricate vertically aligned graphitic carbon nanosheets and their metal carbide hybrids for superior lithium ion batteries and water splitting.* 2015. **137**(16): p. 5480-5485.
70. Yan, H., et al., *Phosphorus-modified tungsten nitride/reduced graphene oxide as a high-performance, non-noble-metal electrocatalyst for the hydrogen evolution reaction.* 2015. **127**(21): p. 6423-6427.
71. Chen, W.F., et al., *Hydrogen-evolution catalysts based on non-noble metal nickel–molybdenum nitride nanosheets.* 2012. **51**(25): p. 6131-6135.
72. Mendoza-Garcia, A., et al., *Controlled Anisotropic Growth of Co-Fe-P from Co-Fe-O Nanoparticles.* 2015. **127**(33): p. 9778-9781.
73. Prins, R. and M.E.J.C.l. Bussell, *Metal phosphides: preparation, characterization and catalytic reactivity.* 2012. **142**(12): p. 1413-1436.
74. Xing, Z., et al., *Closely interconnected network of molybdenum phosphide nanoparticles: a highly efficient electrocatalyst for generating hydrogen from water.* 2014. **26**(32): p. 5702-5707.
75. Yang, J., et al., *Porous Molybdenum Phosphide Nano-Octahedrons Derived from Confined Phosphorization in UIO-66 for Efficient Hydrogen Evolution.* 2016. **128**(41): p. 13046-13050.
76. Sun, H., et al., *Self-supported transition-metal-based electrocatalysts for hydrogen and oxygen evolution.* 2020. **32**(3): p. 1806326.
77. Tackett, B.M., W. Sheng, and J.G.J.J. Chen, *Opportunities and challenges in utilizing metal-modified transition metal carbides as low-cost electrocatalysts.* 2017. **1**(2): p. 253-263.
78. Wu, A., et al., *Effective electrocatalytic hydrogen evolution in neutral medium based on 2D MoP/MoS2 heterostructure nanosheets.* 2019. **11**(29): p. 25986-25995.
79. Zhang, X., et al., *Molybdenum phosphide/carbon nanotube hybrids as pH-universal electrocatalysts for hydrogen evolution reaction.* 2018. **28**(16): p. 1706523.

80. Cheng, H., et al., *Molybdenum carbide nanodots enable efficient electrocatalytic nitrogen fixation under ambient conditions.* 2018. **30**(46): p. 1803694.
81. Xiao, X., et al., *Salt-templated synthesis of 2D metallic MoN and other nitrides.* 2017. **11**(2): p. 2180-2186.
82. Zhang, J., Q. Zhang, and X.J.A.M. Feng, *Support and interface effects in water-splitting electrocatalysts.* 2019. **31**(31): p. 1808167.
83. He, L., et al., *Molybdenum carbide-oxide heterostructures: in situ surface reconfiguration toward efficient electrocatalytic hydrogen evolution.* 2020. **132**(9): p. 3572-3576.
84. Wu, A., et al., *Hierarchical MoS 2@ MoP core–shell heterojunction electrocatalysts for efficient hydrogen evolution reaction over a broad pH range.* 2016. **8**(21): p. 11052-11059.
85. Chen, C., et al., *Trapping [PMo 12 O 40] 3− clusters into pre-synthesized ZIF-67 toward Mo x Co x C particles confined in uniform carbon polyhedrons for efficient overall water splitting.* 2018. **9**(21): p. 4746-4755.
86. Liu, Q., et al., *Hierarchical nanorods of MoS2/MoP heterojunction for efficient electrocatalytic hydrogen evolution reaction.* 2020. **16**(32): p. 2002482.
87. Gao, Q., et al., *Noble-Metal-Free Electrocatalysts: Structural Design and Electronic Modulation of Transition-Metal-Carbide Electrocatalysts toward Efficient Hydrogen Evolution (Adv. Mater. 2/2019).* 2019. **31**(2): p. 1970009.
88. Jin, H., et al., *Emerging two-dimensional nanomaterials for electrocatalysis.* 2018. **118**(13): p. 6337-6408.
89. Yin, H., et al., *2D Electrocatalysts for Converting Earth-Abundant Simple Molecules into Value-Added Commodity Chemicals: Recent Progress and Perspectives.* 2020. **32**(18): p. 1904870.
90. Novoselov, K.J.S., *o. A. Mishchenko, o. A. Carvalho and AC Neto.* 2016. **353**: p. 6298.
91. Xiong, J., et al., *In situ engineering of double-phase interface in Mo/Mo2C heteronanosheets for boosted hydrogen evolution reaction.* 2018. **3**(2): p. 341-348.

92. Jin, H., et al., *Molten salt-directed catalytic synthesis of 2D layered transition-metal nitrides for efficient hydrogen evolution.* 2020. **6**(9): p. 2382-2394.
93. Li, F., et al., *Construction of porous Mo3P/Mo nanobelts as catalysts for efficient water splitting.* 2018. **57**(43): p. 14139-14143.
94. Wang, J., et al., *Universal Access to Two-Dimensional Mesoporous Heterostructures by Micelle-Directed Interfacial Assembly.* 2020. **132**(44): p. 19738-19743.
95. Zhang, X., et al., *A simple synthetic strategy toward defect-rich porous monolayer NiFe-layered double hydroxide nanosheets for efficient electrocatalytic water oxidation.* 2019. **9**(24): p. 1900881.
96. Yan, H., et al., *Holey reduced graphene oxide coupled with an Mo2N–Mo2C heterojunction for efficient hydrogen evolution.* 2018. **30**(2): p. 1704156.
97. Gu, Y., et al., *Two-dimensional porous molybdenum phosphide/nitride heterojunction nanosheets for pH-universal hydrogen evolution reaction.* 2021. **60**(12): p. 6673-6681.
98. Vrubel, H. and X.J.A.C.I.E. Hu, *Molybdenum boride and carbide catalyze hydrogen evolution in both acidic and basic solutions.* 2012. **51**(ARTICLE): p. 12703-12706.
99. McKone, J.R., et al., *Ni–Mo nanopowders for efficient electrochemical hydrogen evolution.* 2013. **3**(2): p. 166-169.
100. Ma, L., et al., *Efficient hydrogen evolution reaction catalyzed by molybdenum carbide and molybdenum nitride nanocatalysts synthesized via the urea glass route.* 2015. **3**(16): p. 8361-8368.
101. Wang, T., et al., *Enhanced electrocatalytic activity of MoP microparticles for hydrogen evolution by grinding and electrochemical activation.* 2015. **3**(8): p. 4368-4373.
102. Yan, H., et al., *Cluster-like molybdenum phosphide anchored on reduced graphene oxide for efficient hydrogen evolution over a broad pH range.* 2016. **52**(61): p. 9530-9533.

103. Yang, F., et al., *Solid-state synthesis of ultra-small freestanding amorphous MoP quantum dots for highly efficient photocatalytic H2 production.* 2021. **406**: p. 126838.
104. Grancha, T., et al., *Synthesis of Polycarboxylate Rhodium (II) Metal–Organic Polyhedra (MOPs) and their use as Building Blocks for Highly Connected Metal–Organic Frameworks (MOFs).* 2021. **60**(11): p. 5729-5733.
105. Tian, Q., et al., *Design of charge transfer channels: defective TiO 2/MoP supported on carbon cloth for solar-light-driven hydrogen generation.* 2021. **8**(8): p. 2017-2026.
106. Park, J.I., et al., *Room-Temperature Synthesis of a Hollow Microporous Organic Polymer Bearing Activated Alkyne IR Probes for Nonradical Thiol-yne Click-Based Post-Functionalization.* 2021. **16**(11): p. 1398-1402.
107. Chandrasekaran, S., et al., *Electronic structure engineering on two-dimensional (2D) electrocatalytic materials for oxygen reduction, oxygen evolution, and hydrogen evolution reactions.* 2020: p. 105080.
108. Yang, J., et al., *Formation of two-dimensional transition metal oxide nanosheets with nanoparticles as intermediates.* 2019. **18**(9): p. 970-976.
109. Chia, X. and M.J.N.C. Pumera, *Characteristics and performance of two-dimensional materials for electrocatalysis.* 2018. **1**(12): p. 909-921.
110. Sun, Y., et al., *Preparation of molybdenum phosphide nanoparticles/nitrogen-phosphorus co-doped carbon nanosheet composites for efficient hydrogen evolution reaction.* 2020. **284**: p. 121182.
111. Wang, L., et al., *Molybdophosphate derived MoP based electrocatalyst as cathode for Sn–H+ battery to generate H2 and electricity simultaneously.* 2019. **277**: p. 602-610.
112. Kong, F., et al., *In-situ electrochemical self-tuning of amorphous nickel molybdenum phosphate to crystal Ni-rich compound for enhanced overall water splitting.* 2019. **430**: p. 218-227.

113. El-Refaei, S.M., et al., *Dual Doping of MoP with M (Mn, Fe) and S to Achieve High Hydrogen Evolution Reaction Activity in Both Acidic and Alkaline Media.* 2021. **13**(20): p. 4392-4402.
114. Wu, Z., et al., *Highly efficient and stable MoP-RGO nanoparticles as electrocatalysts for hydrogen evolution.* 2017. **232**: p. 254-261.
115. Xiao, P., et al., *Energy Environ. Sci. 2014, 7, 2624–2629; b) J. Kibsgaard, TF Jaramillo.* 2014. **53**: p. 14433-14437.
116. Youn, D.H., et al., *Highly active and stable hydrogen evolution electrocatalysts based on molybdenum compounds on carbon nanotube–graphene hybrid support.* 2014. **8**(5): p. 5164-5173.
117. Lee, M.H., D.H. Youn, and J.S.J.A.C.A.G. Lee, *Nanostructured molybdenum Phosphide/N-Doped carbon nanotube-graphene composites as efficient electrocatalysts for hydrogen evolution reaction.* 2020. **594**: p. 117451.
118. Xu, H., et al., *Hierarchical NiMo phosphide nanosheets strongly anchored on carbon nanotubes as robust electrocatalysts for overall water splitting.* 2018. **10**(35): p. 29647-29655.
119. Lin, L., M. Chen, and L.J.M.C.F. Wu, *Hierarchical MoP/NiFeP hybrid hollow spheres as highly efficient bifunctional electrocatalysts for overall water splitting.* 2021. **5**(1): p. 375-385.
120. Wang, X., et al., *A three-dimensional porous MoP@ C hybrid as a high-capacity, long-cycle life anode material for lithium-ion batteries.* 2016. **8**(19): p. 10330-10338.
121. You, B. and Y.J.C. Sun, *Chalcogenide and phosphide solid-state electrocatalysts for hydrogen generation.* 2016. **81**(10): p. 1045-1055.
122. Gong, M. and H.J.N.R. Dai, *A mini review of NiFe-based materials as highly active oxygen evolution reaction electrocatalysts.* 2015. **8**(1): p. 23-39.
123. Zhang, L., et al., *Nanohybrid of carbon quantum dots/molybdenum phosphide nanoparticle for efficient electrochemical hydrogen evolution in alkaline medium.* 2018. **10**(11): p. 9460-9467.

124. Cui, Y., et al., *A comparative study of molybdenum phosphide catalyst for partial oxidation and dry reforming of methane.* 2019. **44**(23): p. 11441-11447.
125. Jiang, E., et al., *MoP-Mo2C quantum dot heterostructures uniformly hosted on a heteroatom-doped 3D porous carbon sheet network as an efficient bifunctional electrocatalyst for overall water splitting.* 2022. **431**: p. 133719.
126. Gao, Y., et al., *Facile synthesis of MoP-Ru2P on porous N, P co-doped carbon for efficiently electrocatalytic hydrogen evolution reaction in full pH range.* 2022. **303**: p. 120879.
127. Sun, D., et al., *One-pot synthesis of N and P Co-doped carbon layer stabilized cobalt-doped MoP 3D porous structure for enhanced overall water splitting.* 2022. **895**: p. 162595.
128. Anjum, M.A.R. and J.S.J.A.C. Lee, *Sulfur and nitrogen dual-doped molybdenum phosphide nanocrystallites as an active and stable hydrogen evolution reaction electrocatalyst in acidic and alkaline media.* 2017. **7**(4): p. 3030-3038.
129. Wang, L., et al., *Enhanced dielectric tunability and energy storage properties of plate-like Ba0. 6Sr0. 4TiO3/poly (vinylidene fluoride) composites through texture arrangement.* 2018. **158**: p. 112-120.
130. Chen, T., et al., *Fabrication of cerium-doped CoMoP/MoP@ C heterogeneous nanorods with high performance for overall water splitting.* 2021. **35**(17): p. 14169-14176.
131. Zhang, L., et al., *Nanocarbon encapsulating Ni-doped MoP/graphene composites for highly improved electrocatalytic hydrogen evolution reaction.* 2021. **26**: p. 100792.
132. Li, N., et al., *Correction: Co–Mo–P carbon nanospheres derived from metal–organic frameworks as a high-performance electrocatalyst towards efficient water splitting.* 2021. **9**(9): p. 5868-5868.
133. Xu, Y., et al., *Facile fabrication of molybdenum compounds (Mo2C, MoP and MoS2) nanoclusters supported on N-doped reduced graphene oxide for highly efficient hydrogen evolution reaction over broad pH range.* 2021. **417**: p. 129233.

134. Chen, Z., et al., *Facile Synthesis of MoP-RuP2 with Abundant Interfaces to Boost Hydrogen Evolution Reactions in Alkaline Media.* 2021. **11**(9): p. 2347.
135. Li, J., et al., *Template-free fabrication of MoP nanoparticles encapsulated in N-doped hollow carbon spheres for efficient alkaline hydrogen evolution.* 2021. **416**: p. 127677.
136. Yu, H., et al., *Self-supported nanotubular MoP electrode for highly efficient hydrogen evolution via water splitting.* 2019. **127**: p. 1-4.
137. Wang, F., et al., *Increased nucleation sites in nickel foam for the synthesis of MoP@ Ni3P/NF nanosheets for bifunctional water splitting.* 2019. **481**: p. 1403-1411.
138. Jiang, Y., et al., *A hierarchical MoP nanoflake array supported on Ni foam: a bifunctional electrocatalyst for overall water splitting.* 2018. **2**(5): p. 1700369.
139. Du, C., et al., *Hierarchical MoP/Ni 2 P heterostructures on nickel foam for efficient water splitting.* 2017. **5**(30): p. 15940-15949.
140. Hummers Jr, W.S. and R.E.J.J.o.t.a.c.s. Offeman, *Preparation of graphitic oxide.* 1958. **80**(6): p. 1339-1339.
141. Wang, K., et al., *Nanoscale engineering MoP/Fe2P/RGO toward efficient electrocatalyst for hydrogen evolution reaction.* 2018. **43**(30): p. 13939-13945.
142. Yang, L., et al., *Facile synthesis of one-dimensional MoWP hybrid nanowires and their enhanced electrochemical catalytic activities.* 2020. **741**: p. 137107.
143. Vinila, V., et al., *XRD studies on nano crystalline ceramic superconductor PbSrCaCuO at different treating temperatures.* 2014. **2014**.
144. Feng, Y. and Z.J.I.J.o.A.C.T. Yu, *Molybdenum-based electrocatalysts with nanostructured supports for hydrogen evolution reaction.* 2022.
145. Stankovich, S., et al., *Synthesis of graphene-based nanosheets via chemical reduction of exfoliated graphite oxide.* 2007. **45**(7): p. 1558-1565.
146. Palaniselvam, T., H.B. Aiyappa, and S.J.J.o.M.C. Kurungot, *An efficient oxygen reduction electrocatalyst from graphene by simultaneously generating pores and nitrogen doped active sites.* 2012. **22**(45): p. 23799-23805.

147. Xie, X., et al., *Electrocatalytic hydrogen evolution in neutral pH solutions: dual-phase synergy.* 2019. **9**(9): p. 8712-8718.
148. Khan, R., et al., *3D hierarchical heterostructured LSTN@ NiMn-layered double hydroxide as a bifunctional water splitting electrocatalyst for hydrogen production.* 2021. **285**: p. 119174.
149. Zhang, G.-R., et al., *Cathodic activated stainless steel mesh as a highly active electrocatalyst for the oxygen evolution reaction with self-healing possibility.* 2020. **49**: p. 153-160.
150. Pan, Y., et al., *Core–shell ZIF-8@ ZIF-67-derived CoP nanoparticle-embedded N-doped carbon nanotube hollow polyhedron for efficient overall water splitting.* 2018. **140**(7): p. 2610-2618.
151. Connor, P., et al., *The determination of electrochemical active surface area and specific capacity revisited for the system MnOx as an oxygen evolution catalyst.* 2020. **234**(5): p. 979-994.
152. Deng, Z., et al., *Synthesized ultrathin MoS 2 nanosheets perpendicular to graphene for catalysis of hydrogen evolution reaction.* 2015. **51**(10): p. 1893-1896.